A&A 550, A133 (2013)
DOI: 10.1051/0004-6361/201220053

Astronomy & Astrophysics

Planck intermediate results

VII. Statistical properties of infrared and radio extragalactic sources from the *Planck* Early Release Compact Source Catalogue at frequencies between 100 and 857 GHz⋆,⋆⋆

Planck Collaboration: P. A. R. Ade[85], N. Aghanim[60], F. Argüeso[20], M. Arnaud[74], M. Ashdown[71,6], F. Atrio-Barandela[18], J. Aumont[60], C. Baccigalupi[84], A. Balbi[37], A. J. Banday[89,9], R. B. Barreiro[68], E. Battaner[91], K. Benabed[61,88], A. Benoît[58], J.-P. Bernard[9], M. Bersanelli[35,51], M. Bethermin[74], R. Bhatia[7], A. Bonaldi[70], J. R. Bond[8], J. Borrill[13,86], F. R. Bouchet[61,88], C. Burigana[50,33], P. Cabella[38], J.-F. Cardoso[75,1,61], A. Catalano[76,73], L. Cayón[31], A. Chamballu[56], R.-R. Chary[57], X. Chen[57], L.-Y Chiang[64], P. R. Christensen[81,39], D. L. Clements[56], S. Colafrancesco[47], S. Colombi[61,88], L. P. L. Colombo[23,69], A. Coulais[73], B. P. Crill[69,82], F. Cuttaia[50], L. Danese[84], R. J. Davis[70], P. de Bernardis[34], G. de Gasperis[37], G. de Zotti[46,84], J. Delabrouille[1], C. Dickinson[70], J. M. Diego[68], H. Dole[60,59], S. Donzelli[51], O. Doré[69,10], U. Dörl[79], M. Douspis[60], X. Dupac[42], G. Efstathiou[65], T. A. Enßlin[79], H. K. Eriksen[66], F. Finelli[50], O. Forni[89,9], P. Fosalba[62], M. Frailis[48], E. Franceschi[50], S. Galeotta[48], K. Ganga[1], M. Giard[89,9], G. Giardino[43], Y. Giraud-Héraud[1], J. González-Nuevo[68,84], K. M. Górski[69,92], A. Gregorio[36,48], A. Gruppuso[50], F. K. Hansen[66], D. Harrison[65,71], S. Henrot-Versillé[72], C. Hernández-Monteagudo[12,79], D. Herranz[68], S. R. Hildebrandt[10], E. Hivon[61,88], M. Hobson[6], W. A. Holmes[69], T. R. Jaffe[89,9], A. H. Jaffe[56], T. Jagemann[42], W. C. Jones[26], M. Juvela[25], E. Keihänen[25], T. S. Kisner[78], R. Kneissl[41,7], J. Knoche[79], L. Knox[28], M. Kunz[17,60,3], N. Kurinsky[24], H. Kurki-Suonio[25,45], G. Lagache[60], A. Lähteenmäki[2,45], J.-M. Lamarre[73], A. Lasenby[6,71], C. R. Lawrence[69], R. Leonardi[42], P. B. Lilje[66,11], M. López-Caniego[68], J. F. Macías-Pérez[76], D. Maino[35,51], N. Mandolesi[50,5,33], M. Maris[48], D. J. Marshall[74], E. Martínez-González[68], S. Masi[34], M. Massardi[49], S. Matarrese[32], P. Mazzotta[37], A. Melchiorri[34,52], L. Mendes[42], A. Mennella[35,51], S. Mitra[55,69], M.-A. Miville-Deschênes[60,8], A. Moneti[61], L. Montier[89,9], G. Morgante[50], D. Mortlock[56], D. Munshi[85], J. A. Murphy[80], P. Naselsky[81,39], F. Nati[34], P. Natoli[33,4,50], H. U. Nørgaard-Nielsen[16], F. Noviello[70], D. Novikov[56], I. Novikov[81], S. Osborne[87], F. Pajot[60], R. Paladini[57], D. Paoletti[50], B. Partridge[44], F. Pasian[48], G. Patanchon[1], O. Perdereau[72], L. Perotto[76], F. Perrotta[84], F. Piacentini[34], M. Piat[1], E. Pierpaoli[23], S. Plaszczynski[72], E. Pointecouteau[89,9], G. Polenta[4,47], N. Ponthieu[60,53], L. Popa[63], T. Poutanen[45,25,2], G. W. Pratt[74], S. Prunet[61,88], J.-L. Puget[60], J. P. Rachen[21,79], W. T. Reach[90], R. Rebolo[67,14,40], M. Reinecke[79], C. Renault[76], S. Ricciardi[50], T. Riller[79], I. Ristorcelli[89,9], G. Rocha[69,10], C. Rosset[1], M. Rowan-Robinson[56], J. A. Rubiño-Martín[67,40], B. Rusholme[57], A. Sajina[24], M. Sandri[50], G. Savini[83], D. Scott[22], G. F. Smoot[27,78,1], J.-L. Starck[74], R. Sudiwala[85], A.-S. Suur-Uski[25,45], J.-F. Sygnet[61], J. A. Tauber[43], L. Terenzi[50], L. Toffolatti[19,68], M. Tomasi[51], M. Tristram[72], M. Tucci[72], M. Türler[54], L. Valenziano[50], B. Van Tent[77], P. Vielva[68], F. Villa[50], N. Vittorio[37], L. A. Wade[69], B. D. Wandelt[61,88,30], M. White[27], D. Yvon[15], A. Zacchei[48], and A. Zonca[29]

(Affiliations can be found after the references)

Received 19 July 2012 / Accepted 27 November 2012

ABSTRACT

We make use of the *Planck* all-sky survey to derive number counts and spectral indices of extragalactic sources – infrared and radio sources – from the *Planck* Early Release Compact Source Catalogue (ERCSC) at 100 to 857 GHz (3 mm to 350 μm). Three zones (deep, medium and shallow) of approximately homogeneous coverage are used to permit a clean and controlled correction for incompleteness, which was explicitly not done for the ERCSC, as it was aimed at providing lists of sources to be followed up. Our sample, prior to the 80% completeness cut, contains between 217 sources at 100 GHz and 1058 sources at 857 GHz over about 12 800 to 16 550 deg^2 (31 to 40% of the sky). After the 80% completeness cut, between 122 and 452 and sources remain, with flux densities above 0.3 and 1.9 Jy at 100 and 857 GHz. The sample so defined can be used for statistical analysis. Using the multi-frequency coverage of the *Planck* High Frequency Instrument, all the sources have been classified as either dust-dominated (infrared galaxies) or synchrotron-dominated (radio galaxies) on the basis of their spectral energy distributions (SED). Our sample is thus complete, flux-limited and color-selected to differentiate between the two populations. We find an approximately equal number of synchrotron and dusty sources between 217 and 353 GHz; at 353 GHz or higher (or 217 GHz and lower) frequencies, the number is dominated by dusty (synchrotron) sources, as expected. For most of the sources, the spectral indices are also derived. We provide for the first time counts of bright sources from 353 to 857 GHz and the contributions from dusty and synchrotron sources at all HFI frequencies in the key spectral range where these spectra are crossing. The observed counts are in the Euclidean regime. The number counts are compared to previously published data (from earlier *Planck* results, *Herschel*, BLAST, SCUBA, LABOCA, SPT, and ACT) and models taking into account both radio or infrared galaxies, and covering a large range of flux densities. We derive the multi-frequency Euclidean level – the plateau in the normalised differential counts at high flux-density – and compare it to WMAP, *Spitzer* and IRAS results. The submillimetre number counts are not well reproduced by current evolution models of dusty galaxies, whereas the millimetre part appears reasonably well fitted by the most recent model for synchrotron-dominated sources. Finally we provide estimates of the local luminosity density of dusty galaxies, providing the first such measurements at 545 and 857 GHz.

Key words. cosmology: observations – surveys – galaxies: statistics – galaxies: evolution – galaxies: star formation – galaxies: active

⋆ Appendices are available in electronic form at http://www.aanda.org

⋆⋆ Corresponding author: herve.dole@ias.u-psud.fr

1. Introduction

Among other advantages, all-sky multifrequency surveys have the benefit of probing rare and/or bright objects in the sky. One reason to probe bright objects is to study the number counts of extragalactic sources and their spectral shapes. In the far-infrared (FIR) the sources detected by these surveys are usually dominated by low-redshift galaxies with $z < 0.1$, as found by IRAS at 60 μm (Ashby et al. 1996) but a few extreme objects like the lensed F10214 source (Rowan-Robinson et al. 1991) also appear. However, the population in the radio band is dominated by synchrotron sources (in particular, blazars) at higher redshift (see de Zotti et al. 2010, for a recent review). Previous multifrequency all-sky surveys were carried out in the infrared (IR) range by the IRAS satellite (between 12 and 100 μm; Neugebauer et al. 1984), and more recently by AKARI (between 2 and 180 μm; Murakami et al. 2007) and WISE (between 3.4 and 22 μm; Wright et al. 2010). Early, limited sensitivity surveys were carried out in the IR and microwave range by COBE (between 1.2 μm and 1 cm; Boggess et al. 1992), and more recently in the microwave range by WMAP (between 23 and 94 GHz; Bennett et al. 2003; Wright et al. 2009; Massardi et al. 2009; de Zotti et al. 2010).

Planck's all-sky, multifrequency surveys offer several advantages to all of the above. The frequency range covered is wide, extending from 30 to 857 GHz; observations at all frequencies were made simultaneously, reducing the influence of source variability; the calibration is uniform; and the delivered catalogue of sources used in this paper was carefully constructed and validated.

The *Planck* frequency range fully covers the transition between the dust emission dominated regime (tracing star formation), and the synchrotron regime (tracing active galactic nuclei). The statistical analysis of the populations in this spectral range has never been done before. At large flux densities (typically 1 Jy and above), number counts from all-sky surveys of extragalactic FIR sources show a Euclidean component, i.e. a distribution of the number of source per flux density bin S_ν at observed frequency ν ($\mathrm{d}N/\mathrm{d}S_\nu$ in $\mathrm{Jy}^{-1}\,\mathrm{sr}^{-1}$) proportional to $S_\nu^{-2.5}$ (see Eq. (1)). This result is in line with expectations from a local Universe uniformly filled with non-evolving galaxies (Lonsdale & Hacking 1989; Hacking & Soifer 1991; Bertin & Dennefeld 1997; Massardi et al. 2009; Wright et al. 2009). In the radio range, the Euclidean part is modified by the presence of higher-redshift sources. At flux densities smaller than typically 0.1 to 1 Jy, an excess in the number counts compared to the Euclidean level is an indication of evolution in luminosity and/or density of the galaxy populations. This effect is clearly seen in deeper surveys in the FIR (e.g. Genzel & Cesarsky 2000; Dole et al. 2001, 2004; Frayer et al. 2006; Soifer et al. 2008; Bethermin et al. 2010a); in the submillimetre (submm) range (e.g. Barger et al. 1999; Blain et al. 1999; Ivison et al. 2000; Greve et al. 2004; Coppin et al. 2006; Weiss et al. 2009; Patanchon et al. 2009; Clements et al. 2010; Lapi et al. 2011); – and in the millimetre and radio ranges (e.g. de Zotti et al. 2010; Vieira et al. 2010; Vernstrom et al. 2011).

The *Planck*[1] all-sky survey covers nine bands between 30 and 857 GHz. It gives us for the first time robust extragalactic counts over a wide area of sky at these wavelengths, and the first all-sky coverage between 3 mm (WMAP) and 160 μm (AKARI) – e.g. see Table 1 of Planck Collaboration (2011c). The counts in turn give us powerful constraints on the long-wavelength spectral energy distribution (SED) of the dusty galaxies investigated e.g. by IRAS, and on the short-wavelength SED of the active galaxies studied at radio wavelengths, e.g. by WMAP or ground-based facilities.

For *Planck*'s six highest frequency bands (100 to 857 GHz, we present here the extragalactic number counts and spectral indices of galaxies selected at high Galactic latitude and using identifications. *Planck* number counts and spectral indices of extragalactic radio-selected sources were already published for the frequency range 30 to 217 GHz using results from the LFI and HFI instruments (Planck Collaboration 2011d). The transition between synchrotron-dominated sources and thermal dust-dominated occurs in the crucial spectral range 200–800 GHz. Thus our broader frequency data allow a better spectral characterisation of sources.

We use the WMAP 7 year best-fit ΛCDM cosmology (Larson et al. 2011), with $H_0 = 71\ \mathrm{km\,s^{-1}\,Mpc^{-1}}$, $\Omega_\Lambda = 0.734$ and $\Omega_\mathrm{M} = 0.266$.

2. *Planck* data, masks and sources

Planck (Tauber et al. 2010; Planck Collaboration 2011a) is the third generation space mission to measure the anisotropy of the cosmic microwave background (CMB). It observes the sky in nine frequency bands covering 30–857 GHz with high sensitivity and angular resolution from 31′ to 5′. The Low Frequency Instrument LFI; (Mandolesi et al. 2010; Bersanelli et al. 2010; Mennella et al. 2011) covers the 30, 44, and 70 GHz bands with amplifiers cooled to 20 K. The High Frequency Instrument (HFI; Lamarre et al. 2010; Planck HFI Core Team 2011a) covers the 100, 143, 217, 353, 545, and 857 GHz bands with bolometers cooled to 0.1 K. Polarization is measured in all but the highest two bands (Leahy et al. 2010; Rosset et al. 2010). A combination of radiative cooling and three mechanical coolers produces the temperatures needed for the detectors and optics (Planck Collaboration 2011b). Two Data Processing Centers (DPCs) check and calibrate the data and make maps of the sky (Planck HFI Core Team 2011b; Zacchei et al. 2011). *Planck*'s sensitivity, angular resolution, and frequency coverage make it a powerful instrument for galactic and extragalactic astrophysics as well as cosmology. Early astrophysic results are given in Planck Collaboration early result papers (Papers VIII to XXVI), based on data taken between 13 August 2009 and 7 June 2010. Intermediate astrophysics results are now being presented in a series of papers based on data taken between 13 August 2009 and 27 November 2010.

The *Planck* data used in this paper (unlike other intermediate *Planck* papers) come entirely from the Early Release Compact Source Catalogue, or ERCSC (Planck Collaboration 2011c,i). This in turn is based on *Planck*'s first 1.6 sky surveys, data taken between 13 August 2009 and 7 June 2010. First results from the ERCSC are published as *Planck* early papers (Planck Collaboration 2011d–g). In this paper, we use only HFI data, covering the 100–857 GHz range in six bands.

2.1. Galactic masks

To obtain reliable extragalactic number counts, uncontaminated by Galactic sources, we mask out areas of the sky strongly affected by Galactic sources, defining a set of "Galactic masks".

[1] *Planck* (http://www.esa.int/Planck) is a project of the European Space Agency (ESA) with instruments provided by two scientific consortia funded by ESA member states (in particular the lead countries France and Italy), with contributions from NASA (USA) and telescope reflectors provided by a collaboration between ESA and a scientific consortium led and funded by Denmark.

Table 1. Percentage and number of *Planck* source identifications using the SIMBAD and NED databases.

			Galactic							
	Extragal		Insecure		Secure		Unident		Total	
Zone	%	*N*	%	*N*	%	*N*	%	*N*	%	*N*
857 deep	91.2	73	2.5	2	1.2	1	5.0	4	100	80
medium	95.5	255	1.9	5	0.0	0	2.6	7	100	267
shallow	94.6	697	1.6	12	0.8	6	3.0	22	100	737
545 deep	76.5	39	7.8	4	2.0	1	13.7	7	100	51
medium	91.1	143	2.5	4	0.0	0	6.4	10	100	157
shallow	91.8	301	2.1	7	0.9	3	5.2	17	100	328
353 deep	81.6	31	2.6	1	5.3	2	10.5	4	100	38
medium	87.0	94	0.9	1	2.8	3	9.3	10	100	108
shallow	78.0	170	4.6	10	4.6	10	12.8	28	100	218
217 deep	77.3	17	0.0	0	22.7	5	0.0	0	100	22
medium	92.5	62	1.5	1	1.5	1	4.5	3	100	67
shallow	88.5	170	0.5	1	4.2	8	6.8	13	100	192
143 deep	86.7	13	0.0	0	13.3	2	0.0	0	100	15
medium	100.0	48	0.0	0	0.0	0	0.0	0	100	48
shallow	96.8	182	0.5	1	1.6	3	1.1	2	100	188
100 deep	77.8	14	0.0	0	22.2	4	0.0	0	100	18
medium	100.0	45	0.0	0	0.0	0	0.0	0	100	45
shallow	93.9	154	0.0	0	3.7	6	2.4	4	100	164

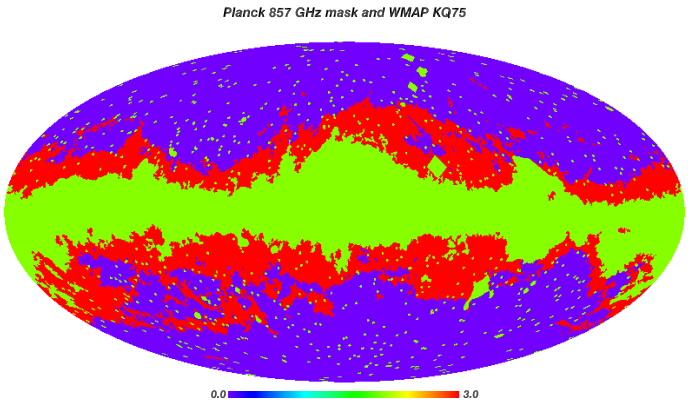

Fig. 1. Comparison between our *Planck* 857 GHz mask (red indicates regions removed from the analysis) and the WMAP 7-year KQ75 mask (green means removed); unlike the case for the mask employed in this paper, the WMAP mask excludes some point sources. The background (blue) is the sky area used for our analysis. This map is a Mollweide projection of the sky in Galactic coordinates.

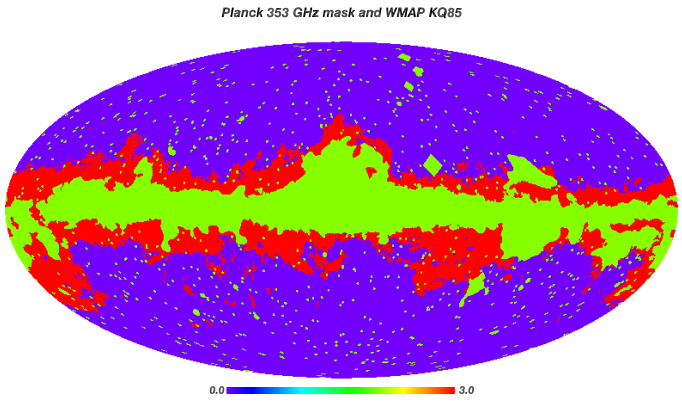

Fig. 2. Comparison between our *Planck* 353 GHz mask (red means removed) and WMAP 7-year KQ85 mask (green). The background (blue) is the sky area used for the analysis.

These are based on removing a fraction of the sky above a specified level in sky surface brightness. We use two masks, one at high frequencies (857 and 545 GHz), and one at lower frequencies (353 GHz and below). The use of two different masks is motivated by the different astrophysical components dominating the higher HFI frequencies and the lower frequencies, which are not necessarily spatially correlated. While emission from Galactic dust dominates at 857 GHz, its spectrum decreases with decreasing frequency. On the contrary, the synchrotron and free-free components dominate at 100 GHz.

Before applying a brightness cut to the maps, we degrade the angular resolution of the maps from 1.′5 ($N_{\rm side}$ = 2048 in HEALPIX; Górski et al. 2005) down to 55′ ($N_{\rm side}$ = 64). The maps at low resolution are then interpolated at the original high angular resolution. Creating a Galactic mask using this procedure has the double benefit of: 1) not masking the bright sources (because they are smoothed away); and 2) smoothing the Galactic structure. We checked to make sure that even the brightest sources remained unmasked after applying this smoothing.

The 857 GHz Galactic mask keeps 48% of the sky for analysis (thus removing 52% of the sky), and this corresponds to a cut of 2.2 MJy sr^{-1} at 857 GHz. This mask is applied at 857 and 545 GHz. The 353 GHz Galactic mask keeps 64% of the sky for analysis (thus removing 36% of the sky), and corresponds to a cut of 0.28 MJy sr^{-1} at 353 GHz.This mask is applied at 353, 217, 143 and 100 GHz.

Figures 1 and 2 show the *Planck* masks, comparing them with the WMAP 7 year KQ75 and KQ85 masks (Gold et al. 2011; Jarosik et al. 2011). Note that we do not use the WMAP masks in this work.

2.2. Three zones in the sky: deep, medium and shallow

Three main zones are identified to ensure reasonably homogeneous coverage of the sky by the *Planck* detectors at each

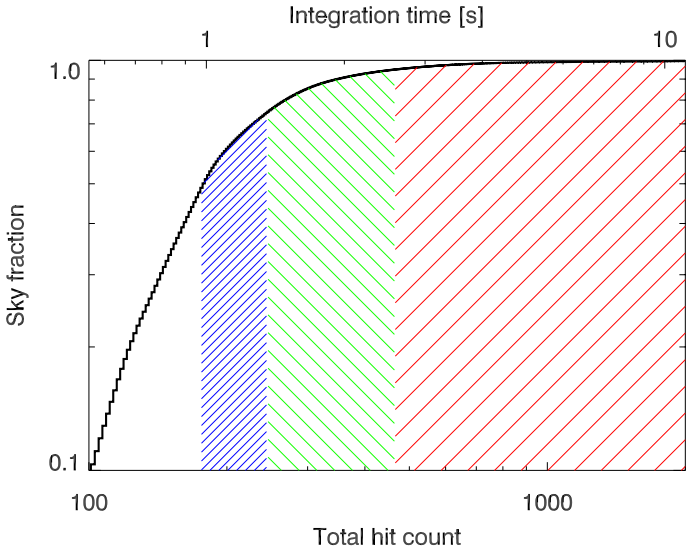

Fig. 3. Cumulative distribution of *Planck* hit counts on the sky (here at 857 GHz with $N_{\rm side}$ = 2048), with the corresponding integration time per sky pixel (given on the top axis). The three sky zones used in the analysis are defined at 857 GHz: shallow (50 to 75% of the hit count distribution, short-spaced lines, blue); medium (75 to 95% of the hit counts, medium-spaced lines, green); and deep (95% and above hits, widely-spaced lines, red).

frequency, thereby allowing a clean and simple estimate of the completeness. As noted above, the *Planck* data used here correspond to approximately 1.6 complete surveys of the sky; in addition each survey has non-uniform coverage of the sky (Planck Collaboration 2011a; Planck HFI Core Team 2011a,b). While performing statistics on sources drawn from a non-uniformly covered survey is feasible, both the nature of the *Planck* data (including scanning strategy, and masking of planets (see the ERCSC article Planck Collaboration 2011c) and its heterogeneous coverage (see Fig. 3) make it difficult to implement. We therefore select three zones in the sky, in each of which the observations are approximatively homogeneous in integration time.

The hit count can be defined by counting the number of times a single *Planck* detector observes one sky position in the sky. The hit count can also be defined for a particular frequency band: it is the number of times each sky pixel has been hit by any *Planck* detector at a given frequency. We will be using this latter definition. This quantity is similar to $N_{\rm obs}$ in WMAP data files.

The three zones have hit counts varying by not more than a factor of two, except in the smaller deep zone (at the ecliptic poles) where there is high redundancy. They are defined as (and illustrated in Fig. 3):

- deep: <5% of the best covered sky fraction (or 95% or more of the cumulative hit count distribution at a given frequency);
- medium: 5 to 25% of the best covered sky fraction (or 75 to 95% of the cumulative hit count distribution at a given frequency);
- shallow: 25 to 50% of the best covered sky fraction (or 50 to 75% of the cumulative hit count distribution at a given frequency).

Thus, pixels in the deep zone (at a given frequency) all have a hit count value greater than or equal to the hit count value corresponding to 95% of the total distribution at this frequency. Note that each frequency map has different hit counts, due to the focal plane geometry; each zone will thus have slight differences in geometry from one frequency to another, leading to slightly different surface areas. Table 2 summarizes the surface area of each zone; typically, the deep zone covers 1000 deg^2, the medium zone about 3000 deg^2, and the shallow about 12 000 deg^2. Figure 4 (or 5) shows the three different zones used in this analysis: deep, medium and shallow at 857 GHz (100 GHz), respectively.

2.3. Sample selection and validation

The sample is drawn from the ERCSC (Planck Collaboration 2011c), which was constructed to contain high SNR sources. Notice that at high frequency, the noise is dominated by the confusion, mainly due to faint extragalactic sources and Galactic cirrus (Condon 1974; Hacking et al. 1987; Franceschini et al. 1989; Helou & Beichman 1990; Franceschini et al. 1991, 1994; Toffolatti et al. 1998; Dole et al. 2003; Negrello et al. 2004; Dole et al. 2006). The selection is performed with the following steps at each HFI frequency independently:

- select sources within each zone: deep, medium and shallow;
- select point sources, using the keyword "EXTENDED" set to zero.

These criteria should favour the presence of galaxies rather than Galactic sources. To validate this, we make three checks in addition to using conservative masks.

1. We measure the mid-IR to submm flux density ratios of known Galactic cold cores (from the *Planck* Early Cold Core catalogue, ECC, Planck Collaboration 2011h) and conversely of known galaxies in the ERCSC. Using WISE (Wright et al. 2010) W3 and W4 bands (when available with the first public release), and the 857 GHz HFI band, we measure a factor of 100 to 200 between the submm-to-mid-infared ratios of galaxies and ECC sources. When measuring this ratio in our sample, we see that the submm-to-mid-infared colours of all sources in our sample are compatible with galaxy colours, and not with ECC colours.
2. The CIRRUS flag in the ERCSC gives an estimate of the normalised neighbour surface density of sources at 857 GHz, as a proxy for cirrus contamination. The median value of the CIRRUS flag in our sample is 0.093 at 857 GHz, a low value compatible with no cirrus contamination when used in conjunction with the EXTENDED=0 flag (e.g. Herranz et al. 2012).
3. We query the NED and SIMBAD databases at the positions of all our ERCSC sources using a 2.′5 search radius. Each *Planck* source has many matches (many of them completely unrelated, e.g. foreground stars), and the identification is more complex at higher frequencies. However, as we show later, our $N(>S)$ cumulative distribution of sources is always less than 200 sources per steradian, i.e. less than 3.3×10^{-4} ERCSC sources per 2.′5 search radius on average. We thus search for the most probable match by identifying the source type in this order: Galactic, then extragalactic. The Galactic types include supernova remnants, planetary nebulae, nebulae, HII regions, stars, molecular clouds, globular/star clusters. We call a source "Galactic unsecure" when one of the two databases returns no identification and the other a Galactic identification. We do not use "Galactic secure" or "Galactic un-secure" sources in the analysis in this paper. The statistics of identifications is given in Table 1.

Our final sample is composed of confirmed galaxies, the vast majority being NGC, IRAS, radio galasy and blazar objects, as

Table 2. Number of extragalactic sources by zone before (after) the completeness cut, and the surface area of the zones.

ν	N Before (After) completeness cut				Surface area [deg^2]			
[GHz]	Deep	Medium	Shallow	Total	Deep	Medium	Shallow	Total
857	77 (24)	262 (115)	719 (313)	1058 (452)	880	2288	9800	12 969
545	46 (8)	153 (69)	318 (143)	517 (220)	874	2324	9551	12 749
353	35 (14)	104 (59)	198 (151)	337 (224)	1086	2971	12 373	16 431
217	17 (15)	65 (57)	183 (71)	265 (143)	1104	3169	11 900	16 174
143	13 (8)	48 (44)	184 (90)	245 (142)	1111	2972	11 977	16 061
100	14 (6)	45 (39)	158 (77)	217 (122)	1072	2870	12 611	16 554

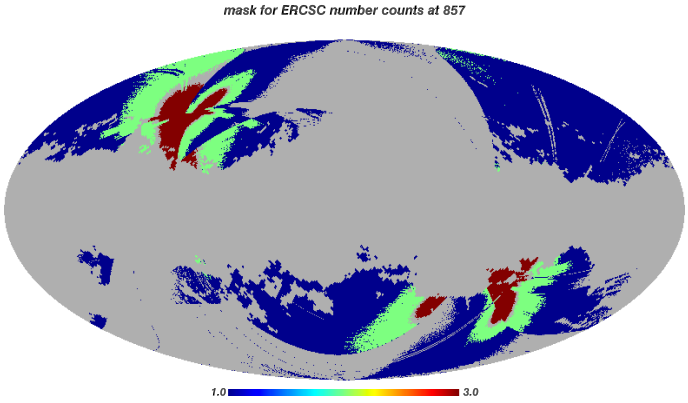

Fig. 4. The three sky zones used in the analysis at 857 GHz: deep (red); medium (green); and shallow (blue). These are based on the 857 GHz hit counts.

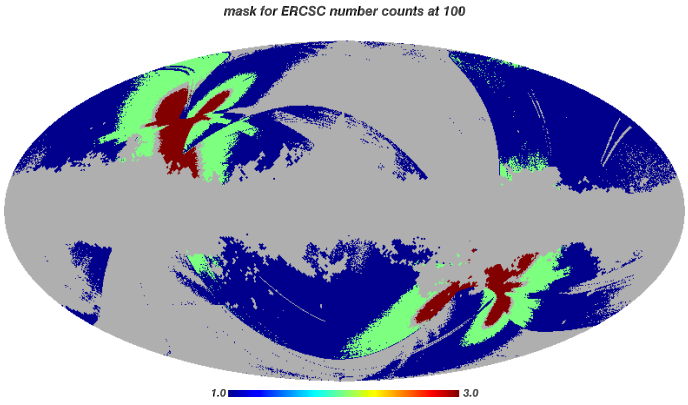

Fig. 5. The three sky zones used in the analysis at 100 GHz: deep (red); medium (green); and shallow (blue). These are based on the 100 GHz hit counts.

well as some unidentified sources (a small fraction of the total number). The few completely unidentified sources, where no SIMBAD or NED ID was found, are interpreted as potential galaxies, and hence are included in our counts, because they have a small cirrus flag value (see point 2 above). Their relatively small number don't change the results presented in this article, wether or not we include these sources.

Table 2 summarises the source number and surface area of each zone (deep, medium and shallow). We find a total number of sources ranging from 217 at 100 GHz to 1058 at 857 GHz.

2.4. Completeness

The ERCSC Pipeline (Planck Collaboration 2011c) used extensive Monte Carlo simulations (to account for systematic and sky

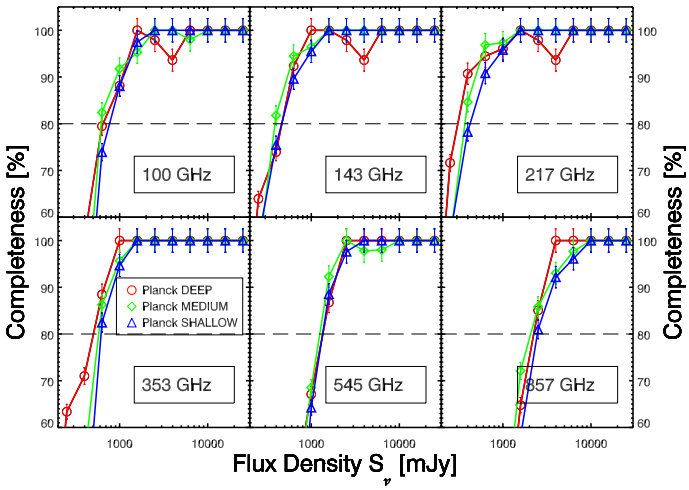

Fig. 6. Completeness (vs. flux density of sources) coming from the Monte Carlo runs for the ERCSC and derived for each zone. The horizontal dashed line represents our threshold for number count analysis.

noise) to assess various parameters such as positional or flux density accuracies. Here, we use the results of those runs to estimate the completeness in each of the three zones, as presented in Fig. 6. The uncertainties in completeness are at the 5% level, as discussed in Planck Collaboration (2011c) and Planck Collaboration (2011i). The correction for incompleteness is then applied to the number counts of each zone separately.

We use a completeness level threshold of 80% for all frequencies. This ensures: 1) minimal source contamination; 2) no photometric biases (Planck Collaboration 2011i); and 3) good photometric accuracy (Planck Collaboration 2011i) – see Sect. 2.5. The number of sources actually used to estimate the number counts is given in Table 3, which also includes the number of unidentified sources. In the end, we use a number of sources ranging from 122 at 100 GHz to 452 at 857 GHz (Table 2).

2.5. Photometry

The photometry of the ERCSC is extensively detailed in Planck Collaboration (2011c) as well as in the explanatory supplement Planck Collaboration (2011i). Here we use the "FLUX" field for flux densities. Notice that 100 and 217 GHz flux densities can be affected by Galactic CO lines (Planck HFI Core Team 2011b).

We would like to emphasise that the extensive simulations performed in the process of generating/validating the ERCSC allow us to derive reliable completeness estimates for each zone (see Sect. 2.4) and also to estimate the quality of the photometry. In the faintest flux density bins that we are using

Table 3. Number of extragalactic sources used in the deep (D), medium (M), and shallow (S) number counts, and the corresponding number of unidentified sources.

S_ν [Jy]		$N_{\rm used}/N_{\rm unidentified}$																	
		857 GHz			545 GHz			353 GHz			217 GHz			143 GHz			100 GHz		
		D	M	S	D	M	S	D	M	S	D	M	S	D	M	S	D	M	S
0.398	0.303–0.480	...	...	...	...	...	...	...	...	...	7/0	28/1	92/9	3/0	12/0	81/1	...	...	...
0.631	0.480–0.762	...	...	...	...	...	...	8/0	31/4	83/14	3/0	13/1	34/2	2/0	13/0	43/0	4/0	15/0	68/3
1.000	0.762–1.207	...	...	...	...	...	...	4/0	18/2	38/ 7	4/0	8/0	21/1	4/0	10/0	25/0	4/0	11/0	47/1
1.585	1.207–1.913	...	...	...	5/0	26/6	78/9	1/1	6/0	14/ 0	1/0	4/0	11/0	2/0	4/0	12/0	2/0	7/0	13/0
2.512	1.913–3.032	11/0	31/1	139/4	0/0	20/1	28/1	1/0	2/0	8/ 0	...	1/0	3/0	...	3/0	5/0	...	3/0	11/0
3.981	3.032–4.805	7/0	33/2	95/4	1/0	16/1	20/1	...	1/0	6/ 0	...	2/0	1/0	...	1/0	3/0	...	2/0	3/0
6.310	4.805–7.615	3/0	22/2	41/7	1/0	6/0	8/1	...	...	...	...	1/0	1/0	...	1/0	1/0	...	...	2/0
10.000	7.615–12.069	2/0	20/1	23/1	1/0	1/0	5/0	...	1/0	...	...	...	...	...	...	...	...	1/0	1/0
15.849	12.069–22.801	1/0	9/0	15/0	0/0	0/0	4/0	...	...	2/ 0	...	...	...	...	...	...	...	...	...

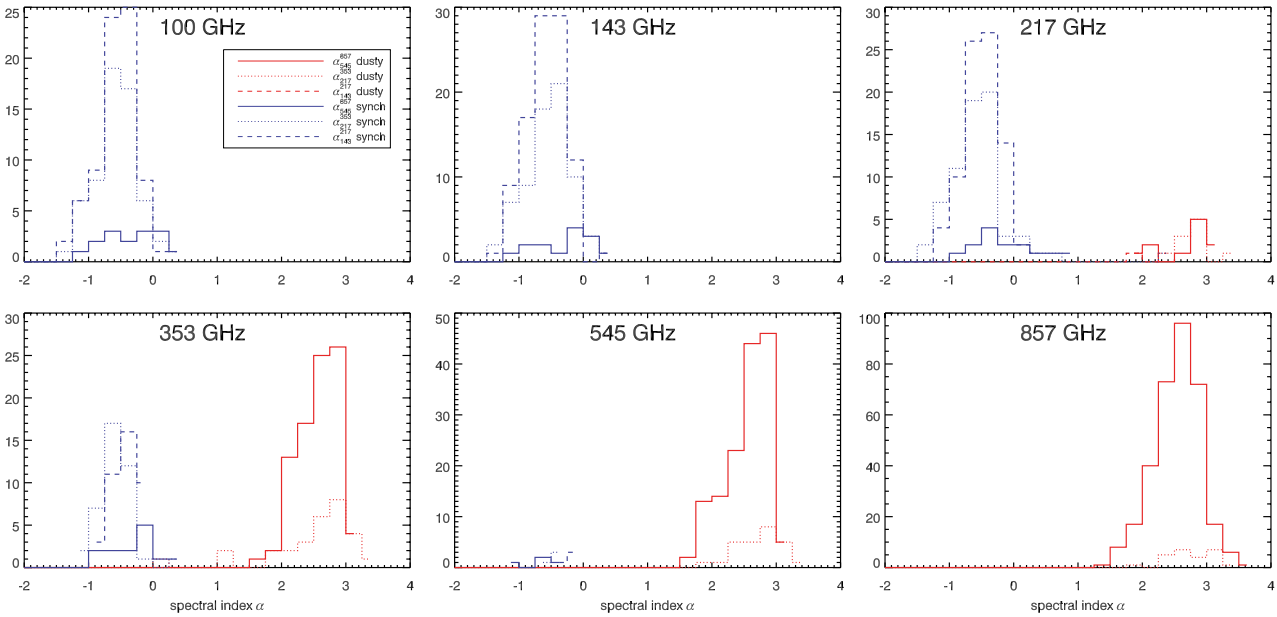

Fig. 7. Distribution of spectral indices (for the sources present in the ERCSC at a given frequency in our sample with completeness of 80% or above). Here α_{143}^{217} is shown as a dotted line, α_{217}^{353} as a dashed line, and α_{545}^{857} as a solid line. The region $2 \leq \alpha \leq 4$ is typical of thermal dust emission. In red we show the dusty sources, whereas in blue we show the synchrotron sources. The sources in all three samples (deep, medium, and shallow) are combined here. Note that, as expected, the 100 GHz, and 143 GHz samples are dominated by radio galaxies, whereas the 545 GHz and 857 GHz samples are dominated by dusty galaxies. At 217 GHz and 353 GHz we observe the transition between the two populations, with significant numbers of both types being present in the samples.

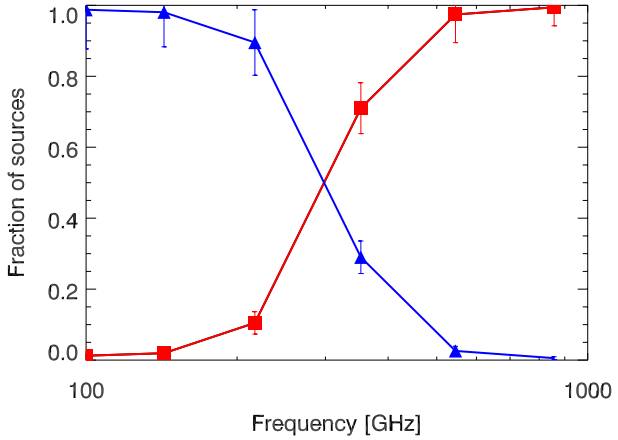

Fig. 8. Fraction of galaxy types as a function of frequency, on the sample having completeness of 80% and above: dusty (red squares) and synchrotron (blue triangles). Error bars are Poissonian.

(corresponding to 80% completeness), there is no photometric offset, and the photometric accuracy from the Monte Carlo simulations (Planck Collaboration 2011i, ; Fig. 7 for reference) is about: 35% at 480 mJy for 100 GHz; 30% at 300 mJy for 143 GHz; 20% at 300 mJy for 217 GHz; 20% at 480 mJy for 353 GHz; 20% at 1207 mJy for 545 GHz; and 20% at 1913 mJy for 857 GHz. This scatter in the faintest flux density bins strongly decreases at larger flux densities. Note that photometric uncertainties can bias the determination of the counts slope (e.g. Murdoch et al. 1973); at our completeness level, the effect is negligible.

From our sample, we also create "Band-filled catalogues". For each frequency/zone sample, we take each source position from the ERCSC and perform aperture photometry from the corresponding images in the other frequencies. We adopt 4σ as the detection threshold. These aperture photometry measurements (and upper limits) are used for the spectral classification of sources and in the spectral index determinations, but *not* in

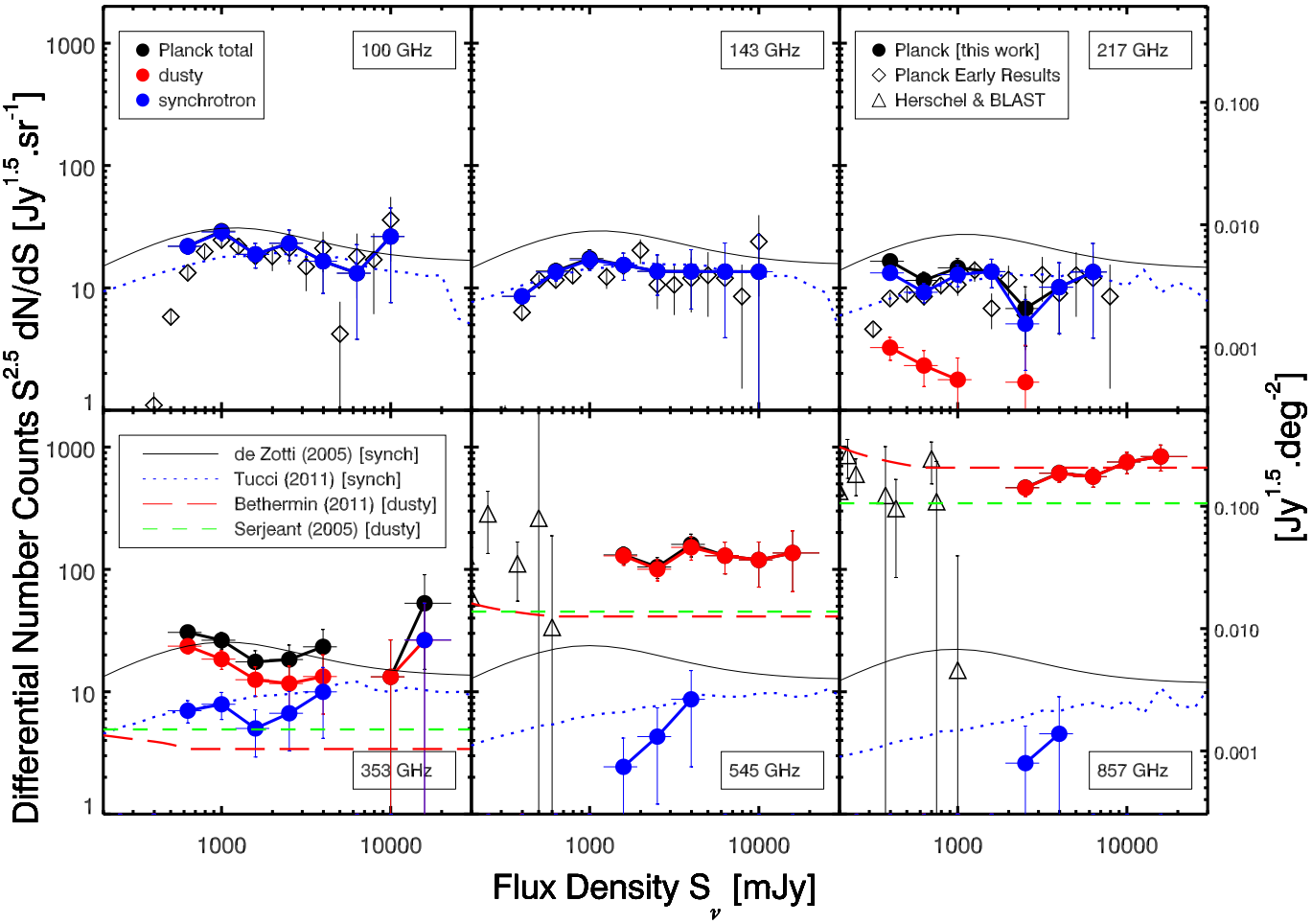

Fig. 9. *Planck* differential number counts, normalised to the Euclidean value (i.e. $S^{2.5}\mathrm{d}N/\mathrm{d}S$), compared with models and other data sets. *Planck* counts: total (black filled circles); dusty (red circles); synchrotron (blue circles). Four models are also plotted: de Zotti et al. (2005, dealing only with synchrotron sources – solid line); Tucci et al. (2011, dealing only with synchrotron sources – dots); Bethermin et al. (2011, dealing only with dusty sources – long dashes); Serjeant & Harrison (2005, dealing only with local dusty sources – short dashes). Other data sets: *Planck* early counts for 30 GHz-selected radio galaxies (Planck Collaboration 2011d) at 100, 143 and 217 GHz (open diamonds); *Herschel* ATLAS and HerMES counts at 350 and 500 μm from Oliver et al. (2010) and Clements et al. (2010); BLAST at the same two wavelengths, from Bethermin et al. (2010b); all shown as triangles. Left vertical axes are in units of $\mathrm{Jy}^{1.5}\ \mathrm{sr}^{-1}$, and the right vertical axis in $\mathrm{Jy}^{1.5}\ \mathrm{deg}^{-2}$.

Table 4. *Planck* number counts at 353, 545, and 857 GHz.

S_ν [Jy]		857 GHz		545 GHz		353 GHz	
		$\frac{\mathrm{d}N}{\mathrm{d}S_\nu}S_\nu^{2.5}$	$N{>}S_\nu$	$\frac{\mathrm{d}N}{\mathrm{d}S_\nu}S_\nu^{2.5}$	$N{>}S_\nu$	$\frac{\mathrm{d}N}{\mathrm{d}S_\nu}S_\nu^{2.5}$	$N{>}S_\nu$
Mean	Range	[$\mathrm{Jy}^{1.5}\ \mathrm{sr}^{-1}$]	[sr^{-1}]	[$\mathrm{Jy}^{1.5}\ \mathrm{sr}^{-1}$]	[sr^{-1}]	[$\mathrm{Jy}^{1.5}\ \mathrm{sr}^{-1}$]	[sr^{-1}]
0.631	0.480–0.762	...	...	...	...	30.6 ± 3.7	50.1 ± 3.3
1.000	0.762–1.207	...	...	...	...	26.4 ± 4.0	21.0 ± 2.1
1.585	1.207–1.913	...	...	131.4 ± 21.4	60.3 ± 4.1	17.6 ± 4.1	8.4 ± 1.3
2.512	1.913–3.032	466.2 ± 70.5	127.7 ± 6.0	104.6 ± 20.4	28.9 ± 2.7	18.3 ± 5.7	4.2 ± 0.9
3.981	3.032–4.805	613.6 ± 96.6	71.8 ± 4.4	160.2 ± 33.8	16.3 ± 2.1	23.3 ± 9.0	2.0 ± 0.6
6.310	4.805–7.615	573.4 ± 103.4	35.0 ± 3.0	129.4 ± 37.5	6.7 ± 1.3	...	...
10.000	7.615–12.069	755.2 ± 150.3	17.7 ± 2.1	119.5 ± 47.8	2.8 ± 0.9	13.2 ± 13.3	0.6 ± 0.3
15.849	12.069–22.801	837.1 ± 200.5	6.3 ± 1.3	136.2 ± 70.4	1.0 ± 0.5	52.9 ± 37.6	0.4 ± 0.3

the number counts measurements (which rely only on ERCSC flux densities). We define the spectral index α by $S_\nu \propto \nu^\alpha$.

The derived spectral indices are used to determine the colour correction of the ERCSC flux densities (Planck HFI Core Team 2011b). This correction changes the flux densities by at most 5% at 857 GHz, 15% at 545 GHz, 14% at 353 GHz, 12% at 217 GHz, and 1% at 143 GHz and 100 GHz.

3. Classification of galaxies into dusty or synchrotron categories

For the purposes of this paper, we aim for a basic classification based on SEDs that separates sources into those dominated by thermal dust emission and those dominated by synchrotron emission. (Free-free emission does exist, but is not dominant,

Table 5. *Planck* number counts at 100, 143, and 217 GHz.

S_ν [Jy]		217 GHz		143 GHz		100 GHz	
		$\frac{dN}{dS_\nu} S_\nu^{2.5}$	$N{>}S_\nu$	$\frac{dN}{dS_\nu} S_\nu^{2.5}$	$N{>}S_\nu$	$\frac{dN}{dS_\nu} S_\nu^{2.5}$	$N{>}S_\nu$
Mean	Range	[Jy$^{1.5}$ sr^{-1}]	[sr^{-1}]	[Jy$^{1.5}$ sr^{-1}]	[sr^{-1}]	[Jy$^{1.5}$ sr^{-1}]	[sr^{-1}]
0.398	0.303–0.480	16.5 ± 2.0	54.3 ± 3.54	8.5 ± 1.1	44.3 ± 2.95	...	...
0.631	0.480–0.762	11.5 ± 1.9	23.0 ± 2.21	13.7 ± 2.1	28.1 ± 2.46	21.9 ± 3.0	43.7 ± 3.14
1.000	0.762–1.207	14.6 ± 2.8	12.0 ± 1.58	17.4 ± 3.1	15.0 ± 1.77	29.1 ± 4.4	22.9 ± 2.22
1.585	1.207–1.913	13.6 ± 3.6	5.1 ± 1.01	15.4 ± 3.8	6.7 ± 1.17	18.8 ± 4.3	9.1 ± 1.35
2.512	1.913–3.032	6.8 ± 3.4	1.8 ± 0.61	13.6 ± 5.0	3.1 ± 0.79	23.2 ± 6.5	4.6 ± 0.95
3.981	3.032–4.805	10.1 ± 5.9	1.0 ± 0.45	13.6 ± 6.9	1.4 ± 0.54	16.5 ± 7.5	1.8 ± 0.59
6.310	4.805–7.615	13.5 ± 9.6	0.4 ± 0.29	13.6 ± 9.7	0.6 ± 0.35	13.2 ± 9.4	0.8 ± 0.40
10.000	7.615–12.069	...	...	13.6 ± 13.6	0.2 ± 0.20	26.3 ± 18.7	0.4 ± 0.28

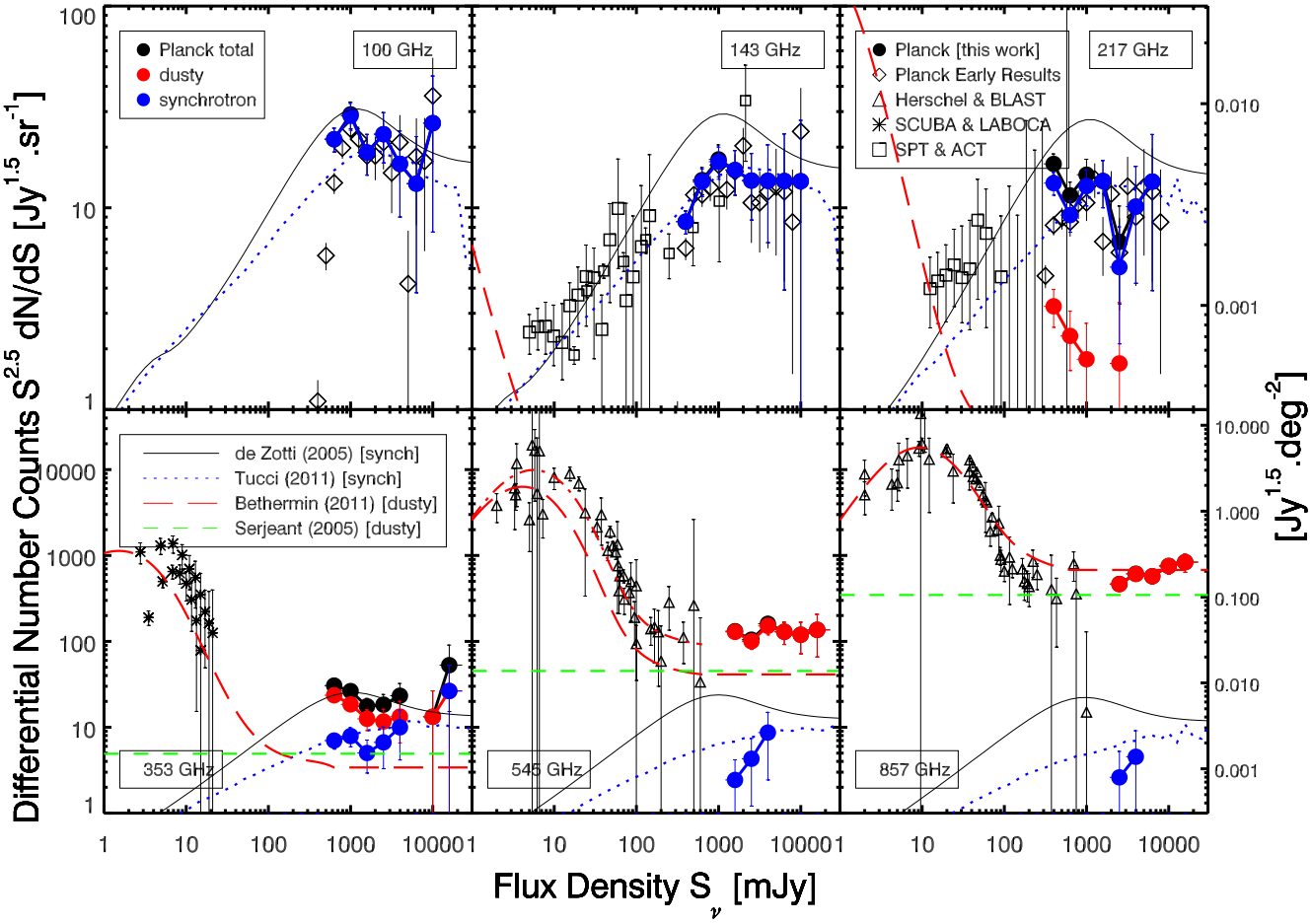

Fig. 10. Same as Fig. 9, but on a wider flux density scale and with the addition of ACT (Marriage et al. 2011) and SPT (Vieira et al. 2010) data shown as squares at 143 and 217 GHz, and SCUBA and LABOCA data shown as stars at 353 GHz (Borys et al. 2003; Coppin et al. 2006; Scott et al. 2006; Beelen et al. 2008; Weiss et al. 2009). Notice that we added the model of Bethermin et al. (2011) at 500 μm (dash-dot) to comply with the *Herschel* data taken at that wavelength (and not at 545 GHz).

e.g., Peel et al. 2011). In order to classify our sources by type, we start with the band-filled catalogues discussed in Sect. 2.5. Thermal dust emission is expected to show spectral indices in the range $\alpha \sim 2$–4. On the other hand, colder temperature sources can show lower α_{545}^{857}, if the 857 GHz measurement falls near the spectral peak. Also, the presence of a strong synchrotron component, or perhaps a free-free emission component, would start to flatten the SED below ~353 GHz. With such issues in mind, we have set up the following classification algorithm:

- all sources with $\alpha_{545}^{857} \geq 2$, or $\alpha_{353}^{545} \geq 2$ are assigned a "dusty" classification;
- all sources where both of these spectral indices are lower than 2, including non-detections, are assigned "synchrotron" classification.

The resulting classification is summarised in Fig. 7, showing the spectral index distributions for each type as a function of observed frequency.

However, some sources are difficult to classify, and could be part of an "intermediate dusty" or "intermediate synchrotron" type. These intermediate sources can be defined as follows:

- being dusty (according to our criterion above) but also having $\alpha_{100}^{857} < 1$;

- being synchrotron (according to our criterion above) but also being detected either at 857 or 545 GHz, and undetected at 353 and 217 and 143 GHz, i.e. sources that show both a significant dust component and a strong synchrotron component.

Among the sources included in the number counts analysis, fewer than 10% are classified as "intermediate". This fraction rises significantly if we remove the completeness cut due to the increasing photometric uncertainties at lower flux densities (see Appendix A for details). Examples of both "dusty" or "synchrotron" sources with somewhat unusual SEDs are discussed in Appendix B.

4. *Planck* extragalactic number counts between 100 and 857 GHz

The *Planck* extragalactic number counts (differential, normalised to the Euclidean slope, and completeness-corrected) are presented in Fig. 9 and Tables 4 and 5. They are obtained using a mean of the 3 zones (weighted by the surface area of each zone).

The error budget in the number counts is made up of: (i) Poisson statistics (ii); the 5% uncertainty in the completeness correction (iii); the absolute photometric calibration uncertainty of 2% at and below 353 GHz, and 7% above 545 GHz (Planck HFI Core Team 2011a,b). According to e.g. Eq. (1) of Bethermin et al. (2011), calibration uncertainties produce errors scaling as the 1.5 power in the Euclidean, normalized, differential number counts.

Notice that for our bright counts, the error budget is dominated by sample variance of nearby sources and consequently by small-number statistics. For instance, the small wiggle seen in the counts at the three highest frequencies (seen at 600 mJy at 353 GHz, 4 Jy at 545 GHz and 10 Jy at 857 GHz) is due to a few tens of local NGC sources in the medium zone (see Appendices B and C).

Integral (i.e. cumulative) combined number counts are shown in Fig. 11. Although error bars are highly correlated, these counts provide a useful estimate of the source surface density. The completeness correction is also applied here, and we use the same cuts in flux density as for the differential counts. Tables 4 and 5 also give the $N > S$ values.

5. Further results and discussion

5.1. Nature of the Galaxies at submillimetre and millimetre wavelengths

The change in the nature of sources (synchrotron dominated vs. dusty) with frequency was first observed in the *Planck* data in Planck Collaboration (2011c). Our new sample allows a more precise quantification because of its completeness. The statistics of synchrotron vs. dusty galaxies are summarised in Fig. 8, showing the fraction of galaxy type as a function of frequency. We estimate the uncertainty in the classification to be of the order of 10% (see Appendix A). The striking result is the almost equal contribution of both source types near 300 GHz. The high frequency channels (545 and 857 GHz) are, unsurprisingly, dominated (>90%) by dusty galaxies. The low frequency channels are, unsurprisingly, dominated (>95%) by synchrotron sources at 100 and 143 GHz. At 217 GHz, fewer than 10% of the sources show a dust-dominated SED.

All the sources from our complete sample have an identified spectral type (by construction), and we can compute the number counts separately for synchrotron and dusty galaxies. Figure 9–11 show the differential and integral number counts by type, also given in Tables 6 and 7. We note that at 353 GHz, about two thirds of the number counts are made-up by dusty sources. At 217 GHz (545 GHz) there is a minor contribution (10% or less) of the dusty (synchrotron) sources contributing to the counts. These number counts of extragalactic dusty and synchrotron sources are an important step towards further constraining models of galaxy SED and to including the results in more general models of galaxy evolution (see below).

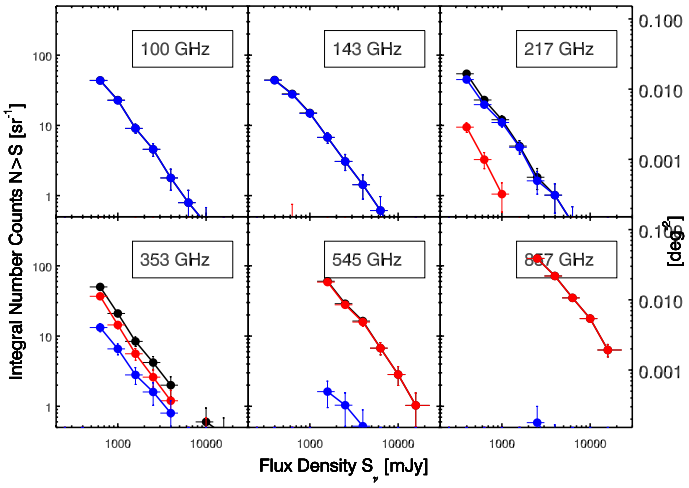

Fig. 11. *Planck* integral number counts (filled circles); dusty (red); synchrotron (blue). Vertical axes are in number per steradian; right axis is in number per square degree. Counts are completeness-corrected. The same faint flux density cut as for differential counts is applied.

5.2. Planck number counts compared with other datasets

The number counts are in fairly good agreement at lower frequencies (100 to 217 GHz) with the counts published in the *Planck* early results, based on a 30 GHz selected sample (Planck Collaboration (2011d); represented as diamonds in Figs. 9 and 10). The effect of incompleteness in the latter is seen in the fainter flux density bins, below about 500 mJy. We also notice a slight disagreement around 400 mJy at 217 GHz, where our counts of synchrotron galaxies exceed the *Planck* early counts by a factor of 1.7 (13.7±1.5 vs. 8.2±0.9 Jy$^{1.5}$ sr^{-1}). This discrepancy can be easily understood: our current selection of synchrotron sources is not the same as the one adopted in the *Planck* Early results paper Planck Collaboration (2011d), in which a more restrictive criterion was used ($\alpha_{143}^{217} < 0.5$). If we adopt the same criterion as in that paper, we find no statistically significant difference between the two estimates of the number counts.

Our estimates of counts also seem consistent with the *Herschel* ATLAS and HerMES counts (Clements et al. 2010; Oliver et al. 2010) at high frequency (545 and 857 GHz) as well as BLAST at the same two wavelengths (Bethermin et al. 2010b), although there is no direct overlap in flux density and small number statistics affect the brightest *Herschel* points.

The ACT 148 GHz data (Marriage et al. 2011) and SPT 150 and 220 GHz (Vieira et al. 2010) data are also plotted in Fig. 10, together with SCUBA and LABOCA data at 353 GHz (Borys et al. 2003; Coppin et al. 2006; Scott et al. 2006; Beelen et al. 2008; Weiss et al. 2009). The ACT and SPT data, when added to the *Planck* data at 143 GHz, cover more than four orders of magnitude in flux density.

Table 6. *Planck* number counts of dusty galaxies at 217, 353, 545, and 857 GHz.

S_ν [Jy]		$\frac{dN}{dS_\nu} S_\nu^{2.5}$ [Jy$^{1.5}$ sr^{-1}]			
Mean	Range	857 GHz	545 GHz	353 GHz	217 GHz
0.398	0.303–0.480	...	...	...	3.2 ± 0.7
0.631	0.480–0.762	...	...	23.6 ± 3.1	2.3 ± 0.8
1.000	0.762–1.207	...	...	18.5 ± 3.2	1.8 ± 0.9
1.585	1.207–1.913	...	129.0 ± 21.1	12.5 ± 3.4	...
2.512	1.913–3.032	463.6 ± 70.2	100.3 ± 19.8	11.7 ± 4.5	1.7 ± 1.7
3.981	3.032–4.805	609.0 ± 6.0	151.5 ± 32.5	13.3 ± 6.7	...
6.310	4.805–7.615	573.4 ± 103.4	129.4 ± 37.5	...	...
10.000	7.615–12.069	755.2 ± 150.3	119.5 ± 47.8	13.2 ± 13.3	...
15.849	12.069–22.801	837.1 ± 200.5	136.2 ± 70.4	26.4 ± 26.5	...

Table 7. *Planck* number counts of synchrotron galaxies at 100, 143, 217, 353, 545, and 857 GHz.

S_ν [Jy]		$\frac{dN}{dS_\nu} S_\nu^{2.5}$ [Jy$^{1.5}$ sr^{-1}]					
Mean	Range	857 GHz	545 GHz	353 GHz	217 GHz	143 GHz	100 GHz
0.398	0.303–0.480	...	...	...	13.3 ± 1.7	8.5 ± 1.1	...
0.631	0.480–0.762	...	...	7.0 ± 1.4	9.2 ± 1.6	13.5 ± 2.1	21.9 ± 3.0
1.000	0.762–1.207	...	...	7.9 ± 2.0	12.8 ± 2.6	16.9 ± 3.1	28.6 ± 4.3
1.585	1.207–1.913	...	2.4 ± 1.7	5.0 ± 2.1	13.6 ± 3.6	15.4 ± 3.8	18.8 ± 4.3
2.512	1.913–3.032	2.6 ± 2.6	4.3 ± 3.1	6.7 ± 3.4	5.1 ± 3.0	13.6 ± 5.0	23.2 ± 6.5
3.981	3.032–4.805	4.5 ± 4.6	8.7 ± 6.2	10.0 ± 5.8	10.1 ± 5.9	13.6 ± 6.9	16.5 ± 7.5
6.310	4.805–7.615	...	...	...	13.5 ± 9.6	13.6 ± 9.7	13.2 ± 9.4
10.000	7.615–12.069	...	...	...	...	13.6 ± 13.6	26.3 ± 18.7
15.849	12.069–22.801	...	...	26.4 ± 26.5	...	...	...

Finally, we checked that our counts are in agreement with the *Planck* Sky Model (Delabrouille et al. 2012).

5.3. Planck number counts and models

5.3.1. Models

Figures 9 and 10 display our present estimates of number counts of extragalactic point sources, based on ERCSC data, together with predictions from recent models of the numbers and evolution of extragalactic sources. These models focus either on radio-selected sources – i.e. sources with spectra dominated by synchrotron radiation at mm/submm wavelengths ("synchrotron sources"): de Zotti et al. (2005) and Tucci et al. (2011) – or on far-IR selected sources – i.e. sources with spectra dominated by thermal cold dust emission at mm/submm wavelengths ("dusty sources"): Serjeant & Harrison (2005) and Bethermin et al. (2011). Many other models exist in the literature, among which are Le Borgne et al. (2009), Negrello et al. (2007), Pearson & Khan (2009), Rowan-Robinson (2009), Valiante et al. (2009), Franceschini et al. (2010), Lacey et al. (2010), Marsden et al. (2011), Wilman et al. (2010), and Rahmati & van Der Werf (2011). A comparison is given with these models in Fig. 12 for 857 GHz.

The de Zotti et al. (2005) model focusses on radio sources, both flat- and steep-spectrum, the latter having a component of dusty spheroidals and GPS (GHz peaked spectrum) sources. It includes cosmological evolution of extragalactic radio sources, based on an analysis of all the main source populations at GHz frequencies. It currently provides a good fit to all data on number counts and on other statistics from ~5 GHz up to ~100 GHz. This model adopts a simple power-law, with a very flat spectral index ($\alpha \simeq -0.1$), for extrapolating the spectra of the brightest extragalactic sources (essentially "blazar[2] sources") to frequencies above 100 GHz.

The Tucci et al. (2011) models provide a description of three populations of radio sources: steep-, flat-, and inverted-spectrum. The flat-spectrum population is further divided into flat-spectrum radio quasars (FSRQ), and BL Lacs. The main novelty of these models is the statistical prediction of the "break" frequency, ν_M, in the spectra of blazar jets modeled by classical, synchrotron-emission physics. The most successful of these models, "C2Ex", assumes different distributions of break frequencies for BL Lac objects and Flat Spectrum Radio Quasars, with the relevant synchrotron emission coming from more compact regions in the jets of the former objects. This model, developed to fit both the Atacama Cosmology Telescope (ACT) data (Marriage et al. 2011) at 148 GHz and the results published in the *Planck* Early paper Planck Collaboration (2011d), is able to give a very good fit to all published data on statistics of extragalactic radio sources: i.e. number counts and spectral index distributions. The model "C2Ex" also correctly predicts the number of blazars observed in the *Herschel* Astrophysical Terahertz Large Area Survey (H-ATLAS) at 600 GHz, as discussed in López-Caniego et al. (2012).

[2] Blazars are jet-dominated extragalactic objects, observed within a small angle of the jet axis and characterized by a highly variable, non-thermal synchrotron emission at GHz frequencies in which the beamed component dominates the observed emission (Angel & Stockman 1980).

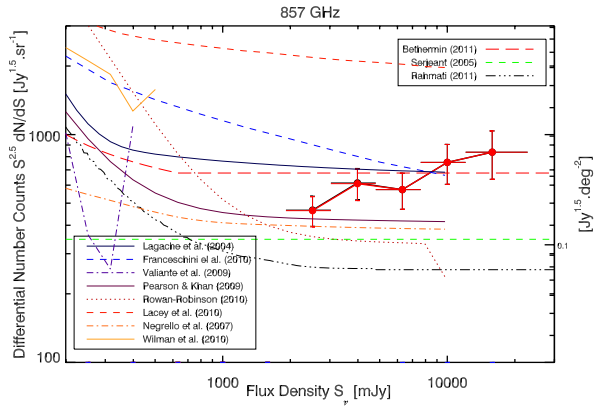

Fig. 12. *Planck* differential number counts at 857 GHz, normalised to the Euclidean (i.e. $S^{2.5}\mathrm{d}N/\mathrm{d}S$). *Planck* counts: total (black filled circles); dusty galaxies (red circles). Models: Bethermin et al. (2011) (long red dashes – dusty); Serjeant & Harrison (2005) (short green dashes – dusty); Rahmati & van Der Werf (2011) (black dash-dot-dot-dot line). Other: Lagache et al. (2004); Negrello et al. (2007); Rowan-Robinson (2009); Valiante et al. (2009); Pearson & Khan (2009); Franceschini et al. (2010); Lacey et al. (2010); Wilman et al. (2010).

The Serjeant & Harrison (2005) model is based on the SED properties of local galaxies detected by IRAS and by SCUBA in the SLUGS sample (Dunne et al. 2000). These local SEDs are used in many models, including the Lapi et al. (2011) model (based on Lapi et al. 2006 and Granato et al. 2004) which links dark matter halo masses with the mass of black holes and the star formation rate.

Bethermin et al. (2011) present a backwards evolution model, taking into account IR galaxies, which is a parametric model fitting the fainter counts. It contains two families of SEDs: normal and starburst, from Lagache et al. (2004).

5.3.2. Synchrotron sources

The de Zotti et al. (2005) model over-predicts the number counts of extragalactic "synchrotron" sources detected by *Planck* at HFI frequencies. The main reason for this disagreement is the spectral "steepening" observed in ERCSC sources above about 70 GHz (Planck Collaboration 2011d,f), and already suggested by other data sets (González-Nuevo et al. 2008; Sadler et al. 2008).

The more recent "C2Ex" model by Tucci et al. (2011) is able to give a reasonable fit to the *Planck* number counts on bright extragalactic radio sources from 100 up to 545 GHz (and marginally at 857 GHz where our data are noisy). However, our current data at 100 and 217 GHz are consistently higher than the model number counts of synchrotron sources in the faintest flux density bin probed by ERCSC completeness-corrected data (300 and 600 mJy, respectively). On the whole, however, the "C2Ex" model accounts well for the observed level of bright extragalactic radio sources up to 545 GHz.

5.3.3. Dusty sources

The Serjeant & Harrison (2005) model performs reasonably well at 857 GHz, but is lower than our observations at 545 and 353 GHz. The Bethermin et al. (2011) model has the same trend – it is compatible with the data at 857 GHz, but is lower than the observations by a factor of about 3 at 353 and 545 GHz. This is likely due to the limits of that model's validity at high flux density (typically above one Jy). For both models, the likely origin of the discrepancy with our new, *Planck*, high-frequency data is the models' inaccurate description of local SEDs. Since the counts of bright sources at high frequency depend mainly on the SED of low-z, IR galaxies, rather than on cosmological evolution at higher redshifts, any discrepancy with models is telling us more about their accuracy in reproducing the averaged SED of the low-z Universe than about any cosmological evolution. This effect is also seen as a discrepancy in the Euclidean level (Sect. 5.4 and Fig. 13).

5.3.4. Other models

Figure 12 shows the predictions of more models at 857 GHz. Most of the models do not explicitly include the counts at such high flux densities (and/or are subject to numerical uncertainties, like Valiante et al. 2009; Wilman et al. 2010). We thus suggest that future model predictions extend up to a few tens of Jy in order to provide a good anchor for the SEDs at low redshift. At 857 GHz, many models disagree with our data, e.g. Negrello et al. (2007), Franceschini et al. (2010), Lacey et al. (2010), Rahmati & van Der Werf (2011), Rowan-Robinson et al. (2010). Other models agree or marginally agree with our data, e.g. Lagache et al. (2004); Pearson & Khan (2009); Bethermin et al. (2011).

5.3.5. Main results

The two main results from the comparison with models are: 1) the good agreement of the Tucci et al. (2011) model with our counts of synchrotron-dominated sources, including for the first time at 353, 545 and marginally at 857 GHz; and 2) the failure of most models to reproduce the dusty-dominated sources between 353 and 857 GHz. This latter point is likely due to errors in the SEDs of local galaxies used (i.e. at redshifts less than 0.1 and flux densities larger than 1 Jy).

5.4. Beyond the number counts

5.4.1. *Planck* observations of the Euclidean level

The Euclidean level of the number counts, described as the plateau level, p, in the normalised differential number counts at high flux density,

$$\mathrm{d}N/\mathrm{d}S = p\,S^{-2.5} \qquad (1)$$

mainly depends on the SED shape of galaxies (local galaxies in the case of high frequency observations).

Figure 13 shows p over more than two orders of magnitude in observed frequency, from the mid-IR to the radio range. The values of p are reported in Table 8. The Euclidean level was determined using number counts above 1 Jy (except in the case of *Spitzer*, where number counts at fainter flux densities were used). Beyond our measurements at *Planck* HFI frequencies (total in black, but also shown by source type: dusty and synchrotron), we also show the *Planck* early results at LFI and HFI 100 GHz frequencies (Planck Collaboration 2011d), as well as WMAP-5year results at Ka (Wright et al. 2009) and in all bands (Massardi et al. 2009; de Zotti et al. 2010), and finally IRAS 25, 60 and 100 μm results (Lonsdale & Hacking 1989; Hacking & Soifer 1991; Bertin & Dennefeld 1997). The *Spitzer* level at 24, 70 and 160 μm comes from counts above 8, 70 and 300 mJy, respectively (Bethermin et al. 2010a). We also plot the models of Serjeant & Harrison (2005) (based on IRAS and SCUBA

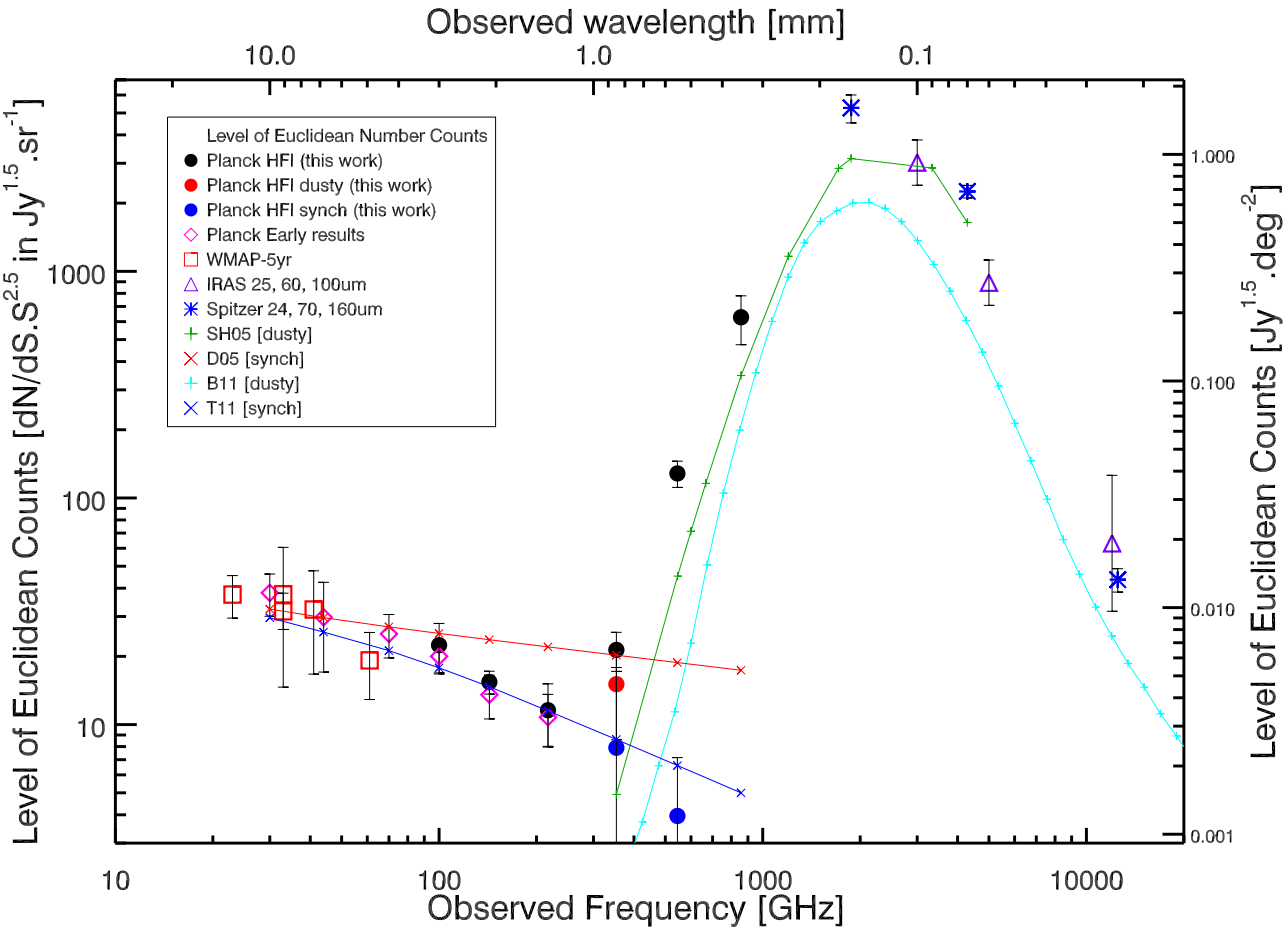

Fig. 13. Euclidean level p (plateau in $S^{2.5}\mathrm{d}N/\mathrm{d}S$, see Eq. (1)) for bright sources, expressed in number of galaxies times $\mathrm{Jy}^{1.5}\,\mathrm{sr}^{-1}$ (or $\mathrm{Jy}^{1.5}\,\mathrm{deg}^{-2}$ on the right axis) averaged between approximately 1 and 3 Jy at microwave to mid-IR frequencies. We specifically show: our *Planck* HFI results (black circles), and separately dusty sources (red circles) and synchrotron sources (blue circles). The dusty 545 GHz point is almost on top of the total *Planck* point. Also shown are: *Planck* Early results (purple diamonds) from (Planck Collaboration 2011d); WMAP-5year (red squares) from Wright et al. (2009); Massardi et al. (2009); de Zotti et al. (2010); IRAS 25, 60 and 100 μm results (purple triangles) from Hacking & Soifer (1991), Lonsdale & Hacking (1989), and Bertin & Dennefeld (1997); and *Spitzer* 24, 70 and 160 μm (blue stars) from Bethermin et al. (2010a). We also plot the models (solid lines): Serjeant & Harrison (2005), based on IRAS and SCUBA data and dealing with dusty galaxies (SH05 green plus signs); Bethermin et al. (2011) (B11 light blue plus signs) dealing with dusty galaxies; de Zotti et al. (2005) (D05 red crosses) dealing with synchrotron sources; Tucci et al. (2011) (T11 blue crosses) for synchrotron sources. Values are given in Table 8.

850 μm local colors), of de Zotti et al. (2005), of Bethermin et al. (2011), and of Tucci et al. (2011).

As expected from our data on number counts discussed above, our current and the early *Planck* estimates are in good agreement at 100 GHz. Also, the *Planck* LFI and WMAP estimates agree within the error bars. The *Planck* contribution is unique in disentangling the dusty from synchrotron sources in the key spectral regime around 300 GHz where the two populations contribute equally to the Euclidean level.

Likewise, the *Planck* measurements of synchrotron sources between 30 and 217 GHz at LFI frequencies and lower HFI frequencies are very well reproduced by the Tucci et al. (2011) model "C2Ex", as is the Euclidean level for synchrotron sources at 353 GHz.

The *Planck* measurements lie above the Serjeant & Harrison (2005) and Bethermin et al. (2011) models at the three upper HFI frequencies between 353 and 857 GHz. There are two explanations for this: (1) the presence of synchrotron galaxies in equal numbers to dusty galaxies between 217 and 353 GHz which are not seen in the IRAS 60 μm selected sample; and (2) the cold dust component in the local Universe. Although the presence of cold dust has been known for some time (Stickel et al. 1998; Dunne et al. 2000), its effects may have been underestimated, as suggested in Planck Collaboration (2011g). There is a significant and largely unexplored cold ($T < 20$ K) component in many nearby galaxies. This excess of submm emission is statistically confirmed here. At 545 GHz for instance, we measure $p = (125 \pm 16)$ $\mathrm{Jy}^{1.5}\,\mathrm{sr}^{-1}$ for the dusty galaxies; the Serjeant & Harrison (2005) model predicts 45 $\mathrm{Jy}^{1.5}\,\mathrm{sr}^{-1}$ (a factor of 2.7 lower) and the Bethermin et al. (2011) predicts 10 $\mathrm{Jy}^{1.5}\,\mathrm{sr}^{-1}$ (a factor of 12 lower). At 353 GHz, we measure $p = 13 \pm 7$ $\mathrm{Jy}^{1.5}\,\mathrm{sr}^{-1}$ for the dusty galaxies, while the Serjeant & Harrison (2005) model predicts 4.92 $\mathrm{Jy}^{1.5}\,\mathrm{sr}^{-1}$ (a factor of 2.7 lower). This is in line with the cooler 60 μm:450 μm colour (i.e., smaller 60/450 flux ratio) found in ERCSC sources (Planck Collaboration 2011g, e.g. their Fig. 4). Unlike the case of the SLUGS sample (Dunne et al. 2000), *Planck* ERCSC sources can have 60 μm: 450 μm flux ratios up to ten times smaller.

5.4.2. Link between the Euclidean level for dusty galaxies and the local luminosity density

In the IR and submm, the bright counts of dusty galaxies probe only the local Universe, which can be approximated as a

Table 8. Values of p, the Euclidean plateau level (in $Jy^{1.5}\ sr^{-1}$) from and *Planck* and other satellite data.

ν [GHz]	p [$Jy^{1.5}\ sr^{-1}$]	Flag	Experiment	Reference
100	22 ± 5	s	*Planck*	PlanckCollab2012
143	15 ± 1	s	*Planck*	PlanckCollab2012
217	11 ± 3	s	*Planck*	PlanckCollab2012
353	21 ± 4	a	*Planck*	PlanckCollab2012
545	128 ± 17	a	*Planck*	PlanckCollab2012
857	627 ± 152	d	*Planck*	PlanckCollab2012
353	15 ± 6	d	*Planck*	PlanckCollab2012
545	125 ± 15	d	*Planck*	PlanckCollab2012
353	7 ± 9	s	*Planck*	PlanckCollab2012
545	3 ± 3	s	*Planck*	PlanckCollab2012
30	38 ± 8	s	*Planck*	PlanckCollab2011
44	29 ± 12	s	*Planck*	PlanckCollab2011
70	25 ± 5	s	*Planck*	PlanckCollab2011
100	20 ± 3	s	*Planck*	PlanckCollab2011
143	13 ± 2	s	*Planck*	PlanckCollab2011
217	10 ± 2	s	*Planck*	PlanckCollab2011
33	31 ± 1	s	WMAP	Wright2009
23	37 ± 7	s	WMAP	Massardi2009
33	37 ± 22	s	WMAP	Massardi2009
41	32 ± 15	s	WMAP	Massardi2009
61	19 ± 6	s	WMAP	Massardi2009
12 000	63 ± 1	d	IRAS	Soifer91Bertin97
5000	891 ± 1	d	IRAS	Soifer91Bertin97
3000	3019 ± 1	d	IRAS	Soifer91Bertin97
12 500	43 ± 5	d	*Spitzer*	Bethermin2010
4285	2252 ± 143	d	*Spitzer*	Bethermin2010
1875	5261 ± 743	d	*Spitzer*	Bethermin2010

Notes. The column "flag" indicates the nature of the sources (a=all; d=dusty; s=synch).

Euclidean space filled with non-evolving populations. The volume $V_{\rm max}$ where a source with a luminosity density L_ν is seen with a flux density larger than $S_{\nu,\rm lim}$ is:

$$V_{\rm max} = \frac{4\pi}{3} D_{\rm max}^3 = \frac{4\pi}{3} \left(\frac{L_\nu}{4\pi S_{\nu,\rm lim}} \right)^{\frac{3}{2}}, \tag{2}$$

where $D_{\rm max}$ is the maximum distance at which a source can be detected, and $S_{\nu,\rm lim}$ the limiting flux density at frequency ν. The contribution of sources with $L_\nu - {\rm d}L_\nu/2 < L_\nu < L_\nu + {\rm d}L_\nu/2$ to the counts is then

$$\frac{{\rm d}N(S_\nu > S_{\nu,\rm lim})}{{\rm d}L_\nu} = \frac{{\rm d}^2N}{{\rm d}L_\nu {\rm d}V} \times \frac{L_\nu^{\frac{3}{2}}}{S_{\nu,\rm lim}^{\frac{3}{2}} 6\sqrt{\pi}}, \tag{3}$$

where $N(S_\nu > S_{\nu,\rm lim})$ is the number of sources brighter than $S_{\nu,\rm lim}$ over the entire sky and $\frac{{\rm d}^2N}{{\rm d}L_\nu {\rm d}V}$ the local luminosity function. The integral counts ${\rm d}N(S_\nu > S_{\nu,\rm lim})/{\rm d}\Omega$ are linked to this local luminosity function by:

$$\frac{{\rm d}N(S_\nu > S_{\nu,\rm lim})}{{\rm d}\Omega} = \frac{1}{4\pi} \int_{L_\nu=0}^{\infty} \frac{{\rm d}^2N}{{\rm d}L_\nu {\rm d}V} \times \frac{L_\nu^{\frac{3}{2}}}{S_{\nu,\rm lim}^{\frac{3}{2}} 6\sqrt{\pi}} \, {\rm d}L_\nu. \tag{4}$$

The differential counts ${\rm d}^2N/({\rm d}S_\nu {\rm d}\Omega)$ are thus

$$\frac{{\rm d}^2N}{{\rm d}S_\nu {\rm d}\Omega} = \frac{S_\nu^{\frac{-5}{2}}}{16\pi^{\frac{3}{2}}} \int_{L_\nu=0}^{\infty} \frac{{\rm d}^2N}{{\rm d}L_\nu {\rm d}V} \times L_\nu^{\frac{3}{2}} \, {\rm d}L_\nu, \tag{5}$$

and the level p of the Euclidean plateau is thus

$$p_\nu = \frac{1}{16\pi^{\frac{3}{2}}} \int_{L_\nu=0}^{\infty} \frac{{\rm d}^2N}{{\rm d}L_\nu {\rm d}V} \times L_\nu^{\frac{3}{2}} \, {\rm d}L_\nu. \tag{6}$$

The local monochromatic luminosity density ρ_ν can be computed as

$$\rho_\nu = \int_{L_\nu=0}^{\infty} \frac{{\rm d}^2N}{{\rm d}L_\nu {\rm d}V} \times L_\nu \, {\rm d}L_\nu. \tag{7}$$

If we assume a single mean color C between frequencies ν_1 and ν_2 (with $S_{\nu_1} = CS_{\nu_2}$) for all the sources, we simply have the relation

$$\frac{\rho_{\nu_2}}{\rho_{\nu_1}} = C. \tag{8}$$

We make this assumption for simplicity. Note, however, that the strongly peaked distributions of spectral indices from Fig. 7 at 857 and 545 GHz are consistent with this assumption. At 353 GHz, the lowest frequency we consider in this analysis, the situation is complicated by the appearance of some synchrotron sources. Their effect, however, is small compared to other uncertainties in the calculation of ρ. If we perform the same analysis on the level of the Euclidean plateau, we obtain

$$\frac{p_{\nu_2}}{p_{\nu_1}} = C^{\frac{3}{2}}. \tag{9}$$

The quantities p_ν and ρ_ν are thus linked by

$$\frac{\rho_{\nu_2}}{\rho_{\nu_1}} = \left(\frac{p_{\nu_2}}{p_{\nu_1}} \right)^{\frac{2}{3}}. \tag{10}$$

We could use ρ_{60} (the IRAS local luminosity density at 60 μm) and p_{60} (the Euclidean level at 60 μm) as a reference, in order to derive ρ_ν, the luminosity density of dusty galaxies at frequency ν (with IRAS as a reference):

$$\rho_\nu = \left(\frac{p_\nu}{p_{60}} \right)^{\frac{2}{3}} \rho_{60}. \tag{11}$$

However, the extrapolation of the dust emission from the FIR to the (sub-)millimetre wavelengths is uncertain (as our data show). We might instead want to use the luminosity density estimated at 850 μm from previous studies, and correct it to account for the excess observed by *Planck*. We can thus use:

$$\rho_\nu = \left(\frac{p_\nu}{p_{850}} \right)^{\frac{2}{3}} \rho_{850}. \tag{12}$$

Both the 60 μm-based and the 850 μm-based estimates are shown in Fig. 14 and discussed in the next section.

5.4.3. Estimate of the local luminosity density for dusty galaxies

We use two reference wavelengths to derive ρ_ν:

- at 60 μm we use IRAS data: ρ_{60} is estimated by Soifer & Neugebauer (1991) and Takeuchi et al. (2006); p_{60} by Soifer & Neugebauer (1991) and Bertin & Dennefeld (1997);
- at 850 μm we use SCUBA SLUGS: ρ_{850} is estimated by Dunne et al. (2000) and Takeuchi et al. (2006); p_{850} by Serjeant & Harrison (2005).

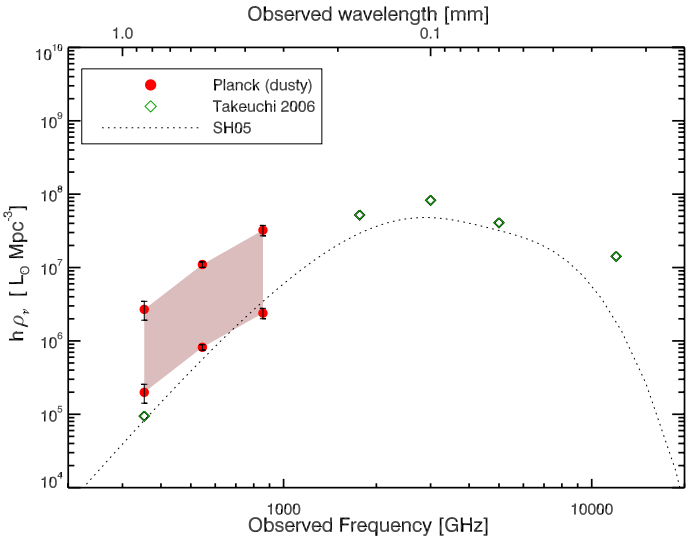

Fig. 14. Luminosity density ρ_ν (in units of $h\ L_\odot\ \mathrm{Mpc}^{-3}$) of dusty galaxies, derived from the Euclidean level p and scaled to the luminosity density of: SCUBA 850 μm data (Dunne et al. 2000; Serjeant & Harrison 2005) (see Eq. (12)); or IRAS 60 μm data (Soifer & Neugebauer 1991; Bertin & Dennefeld 1997; Takeuchi et al. 2003) (see Eq. (11)). Red circles: estimate from *Planck* for dusty galaxies (this work); green diamonds: compilation from Takeuchi et al. (2006); black dots: model from Serjeant & Harrison (2005). Values are given in Table 9. Our *Planck* estimates lie in the shaded area. Note that we take $h = 0.71$ here.

The values from these references are: $\rho_{60} = 4.08 \times 10^7 h\, L_\odot\, \mathrm{Mpc}^{-3}$ and $p_{60} = 891.3\ \mathrm{Jy}^{1.5}\,\mathrm{sr}^{-1}$ at 60 μm; $\rho_{850} = 9.45 \times 10^4 h\, L_\odot\, \mathrm{Mpc}^{-3}$ and $p_{850} = 4.92\ \mathrm{Jy}^{1.5}\,\mathrm{sr}^{-1}$. The use of two reference wavelengths is driven by the oversimplified hypothesis of a constant color C between two frequencies (assumptions described in Sect. 5.4.2). Computing ρ_ν using two different reference wavelengths allows us to estimate the impact of this hypothesis.

The results of our estimated luminosity densities from this simple model are shown in Fig. 14: lower points using the SCUBA 850 μm reference (Eq. (12)); upper points using the IRAS 60 μm reference (Eq. (11)). The values are given in Table 9.

As expected, our *Planck* indirect upper estimate is higher than SLUGS at 353 GHz if we use 850 μm as a reference. This is clearly consistent with our value of p being 2.7 times higher, implying a factor of 2 (i.e. $2.7^{2/3}$) in the luminosity densities. On the other hand, our 353 GHz estimate using 60 μm as a reference falls way above the SCUBA estimate at 850 μm. This again illustrates that caution is required when extrapolating FIR colors to the submm.

The true luminosity density should lie between our lower and upper estimates; the ratio equals 13.5. At 353 GHz, our estimate using SCUBA as a reference should be more appropriate to use than the IRAS extrapolation.

6. Conclusion and summary

From the *Planck* all-sky survey, we derive extragalactic number counts based on the ERCSC (Planck Collaboration 2011c) from 100 to 857 GHz (3 mm to 350 μm). We use an 80% completeness cut on three homogeneous zones, covering a total of about 16 000 deg^2 ($f_{\mathrm{sky}} \sim 0.31$ to 0.40) outside a Galactic mask. We provide, for the first time, bright extragalactic source counts at 353, 545 and 857 GHz (i.e., 850, 550 and 350 μm; see Fig. 9).

Table 9. Values of ρ_ν, the luminosity density of dusty galaxies (in $h\,L_\odot\,\mathrm{Mpc}^{-3}$), inferred from the Euclidean plateau level p and scaled to the luminosity density at 850 μm (upper values) and 60 μm (lower values).

ν [GHz]	ρ_ν [scaled 850 μm] $[h\,L_\odot\,\mathrm{Mpc}^{-3}]$	ρ_ν [scaled 60 μm] $[h\,L_\odot\,\mathrm{Mpc}^{-3}]$
353	$(1.99 \pm 0.57) \times 10^5$	$(2.69 \pm 0.77) \times 10^6$
545	$(8.18 \pm 0.69) \times 10^5$	$(1.10 \pm 0.09) \times 10^7$
857	$(2.39 \pm 0.39) \times 10^6$	$(3.23 \pm 0.52) \times 10^7$

Our counts are in the Euclidean regime, and generally agree with other data sets, when available (Fig. 10).

Using multi-frequency information to classify the sources as dusty- or synchrotron-dominated (and measure their spectral indices), the most striking result is the contribution to the number counts by each population. The cross-over takes place at high frequencies, between 217 and 353 GHz, where both populations contribute almost equally to the number counts. At higher or lower frequencies, counts are quickly dominated by one or other population. We provide for the first time number counts estimates of synchrotron-dominated sources at high frequency (353 to 857 GHz) and dusty-dominated sources at lower frequencies (217 and 353 GHz).

Our counts provide new constraints on models which extend their predictions to bright flux densities. Existing models of synchrotron-dominated sources are not far off from our observations, with the model "C2Ex" of Tucci et al. (2011) performing particularly well at reproducing the synchrotron-dominated source counts up to 545 GHz (and marginally up to 857 GHz, where our statistics become sparse). Perhaps less expected is the failure of most models of dusty sources to reproduce all the high-frequency counts. The model of Bethermin et al. (2011) agrees marginally at 857 GHz but is too low at 545 GHz and at lower frequencies, while the model of Serjeant & Harrison (2005) is marginally lower at 857 GHz, fits the data well at 545 GHz, but is too low at 353 GHz. The likely origin of the discrepancies is an inaccurate description of the SEDs for galaxies at low redshift in these models. Indeed a cold dust component, seen e.g. by Planck Collaboration (2011g), is rarely included in the models at low redshift. This failure to reproduce high-frequency counts at bright flux density should not have any impact on the predictions at fainter flux densities and higher redshifts, as is shown in the good fit to *Herschel* counts. Nevertheless it tells us about the ubiquity of cold dust in the local Universe, at least in statistical terms.

Finally, in Fig. 13, we provide a review of the Euclidean plateau level p of the number counts, spanning nearly three orders of magnitude in both frequency and counts. The values of p are calculated for flux densities above 1 Jy, except in the case of *Spitzer* where fainter objects are used. Figure 13 compares these results with some relevant models. The p value is usually not well reproduced by models (at least for de Zotti et al. 2005; Serjeant & Harrison 2005; Bethermin et al. 2011) in the synchrotron- or dust-dominated regimes. The Tucci et al. (2011) model, on the contrary, reproduces our observations of synchrotron sources, up to 545 GHz. This multifrequency diagnostic is a powerful tool for investigating the SEDs of galaxies in the context of cosmological evolution – at relatively low redshifts for the dusty galaxies. We derive a range of values for the local luminosity density for dusty galaxies, based on simple considerations and using the SCUBA 850 μm and IRAS 60 μm luminosity density as a reference.

The *Planck* multi-frequency all-sky survey is very rich dataset, in particular for extragalactic studies (e.g. Negrello et al. 2012). The final *Planck* catalogue of sources will be based on five complete sky surveys, while the present work is based on only 1.6 surveys. With this improved data set, we expect to provide further constraints on the synchrotron and dust-dominated populations at all frequencies, and over a wider range in redshift.

Acknowledgements. Based on observations obtained with Planck (http://www.esa.int/Planck), an ESA science mission with instruments and contributions directly funded by ESA Member States, NASA, and Canada. The development of Planck has been supported by: ESA; CNES and CNRS/INSU-IN2P3-INP (France); ASI, CNR, and INAF (Italy); NASA and DoE (USA); STFC and UKSA (UK); CSIC, MICINN and JA (Spain); Tekes, AoF and CSC (Finland); DLR and MPG (Germany); CSA (Canada); DTU Space (Denmark); SER/SSO (Switzerland); RCN (Norway); SFI (Ireland); FCT/MCTES (Portugal); and PRACE (EU). This research has made use of the SIMBAD database, operated at CDS, Strasbourg, France. This research has made use of the NASA/IPAC Extragalactic Database (NED) which is operated by the Jet Propulsion Laboratory, California Institute of Technology, under contract with the National Aeronautics and Space Administration. This research has made use of the NASA/ IPAC Infrared Science Archive, which is operated by the Jet Propulsion Laboratory, California Institute of Technology, under contract with the National Aeronautics and Space Administration. This publication makes use of data products from the Wide-field Infrared Survey Explorer, which is a joint project of the University of California, Los Angeles, and the Jet Propulsion Laboratory/California Institute of Technology, funded by the National Aeronautics and Space Administration.

References

Angel, J. R. P., & Stockman, H. S. 1980, ARA&A, 18, 321
Ashby, M. L. N., Hacking, P. B., Houck, J. R., Soifer, B. T., & Weisstein, E. W. 1996, ApJ, 456, 428
Barger, A. J., Cowie, L. L., & Sanders, D. B. 1999, ApJ, 518, L5
Beelen, A., Omont, A., Bavouzet, N., & Kovacs, A 2008, A&A, 485, 645
Bennett, C. L., Halpern, M., Hinshaw, G., et al. 2003, ApJSS, 148, 1
Bersanelli, M., Mandolesi, N., Butler, R. C., et al. 2010, A&A, 520, A4
Bertin, E., & Dennefeld, M. 1997, A&A, 317, 43
Bethermin, M., Dole, H., Beelen, A., & Aussel, H. 2010a, A&A, 512, A78
Bethermin, M., Dole, H., Cousin, M., & Bavouzet, N. 2010b, A&A, 516, A43
Bethermin, M., Dole, H., Lagache, G., Le Borgne, D., & Penin, A. 2011, A&A, 529, A4
Blain, A. W., Kneib, J. P., Ivison, R. J., & Smail, I. 1999, ApJ, 512, L87
Boggess, N. W., Mather, J. C., Weiss, R., et al. 1992, ApJ, 397, 420
Borys, C., Chapman, S., Halpern, M., & Scott, D. 2003, MNRAS, 344, 385
Clements, D. L., Rigby, E., Maddox, S., et al. 2010, A&A, 518, L8
Condon, J. J. 1974, ApJ, 188, 279
Coppin, K., Chapin, E. L., Mortier, A. M. J., et al. 2006, MNRAS, 372, 1621
de Zotti, G., Ricci, R., Mesa, D., et al. 2005, A&A, 431, 893
de Zotti, G., Massardi, M., Negrello, M., & Wall, J. 2010, A&ARv, 18, 1
Delabrouille, J., Betoule, M., Melin, J.-B., et al. 2012, A&A, submitted [arXiv:1207.3675]
Dole, H., Gispert, R., Lagache, G., et al. 2001, A&A, 372, 364
Dole, H., Lagache, G., & Puget, J.-L. 2003, ApJ, 585, 617
Dole, H., Floc'h, E. L., Perez-Gonzalez, P. G., et al. 2004, ApJSS, 154, 87
Dole, H., Lagache, G., Puget, J.-L. et al. 2006, A&A, 451, 417
Dunne, L., Eales, S., Edmunds, M., et al. 2000, MNRAS, 315, 115
Franceschini, A., Toffolatti, L., Danese, L., & De Zotti, G. 1989, ApJ, 344, 35
Franceschini, A., Toffolatti, L., Mazzei, P., Danese, L., & De Zotti, G. 1991, A&AS, 89, 285
Franceschini, A., Mazzei, P., De Zotti, G., & Danese, L. 1994, ApJ, 427, 140
Franceschini, A., Rodighiero, G., & Vaccari, M., 2010, A&A, 517, A74
Frayer, D. T., Fadda, D., Yan, L., et al. 2006, AJ, 131, 250
Genzel, R., & Cesarsky, C. J. 2000, ARA&A, 38, 761
Gold, B., Odegard, N., Weiland, J. L., et al. 2011, ApJSS, 192, 15
González-Nuevo, J., Massardi, M., Argüeso, F., et al. 2008, MNRAS, 384, 711
Górski, K. M., Hivon, E., Banday, A. J., et al. 2005, ApJ, 622, 759
Granato, G. L., de Zotti, G., Silva, L., Bressan, A., & Danese, L. 2004, ApJ, 600, 580
Greve, T. R., Ivison, R. J., Bertoldi, F., et al. 2004, MNRAS, 354, 779
Hacking, P., Houck, J. R., & Condon, J. J. 1987, ApJ, 317, L15
Hacking, P. B., & Soifer, B. T. 1991, ApJ, 367, L49
ESA SP-314 From Ground-Based to Space-Borne Sub-mm Astronomy 1990, ESA, 117
Herranz, D., González-Nuevo, J., Clements, D. L., et al. 2012, A&A, 549, A31
Ivison, R. J., Smail, I., Barger, A. J., et al. 2000, MNRAS, 315, 209
Jarosik, N., Bennett, C. L., Dunkley, J., et al. 2011, ApJSS, 192, 14
Lacey, C. G., Baugh, C. M., Frenk, C. S., et al. 2010, MNRAS, 405, 2
Lagache, G., Dole, H., Puget, J. L., et al. 2004, ApJS, 154, 112
Lamarre, J., Puget, J., Ade, P. A. R., et al. 2010, A&A, 520, A9
Lapi, A., Shankar, F., Mao, J., et al. 2006, ApJ, 650, 42
Lapi, A., Gonzalez-Nuevo, J., Fan, L., et al. 2011, ApJ, 742, 24
Larson, D., Dunkley, J., Hinshaw, G., et al. 2011, ApJS, 192, 16
Le Borgne, D., Elbaz, D., Ocvirk, P., & Pichon, C. 2009, A&A, 504, 727
Leahy, J. P., Bersanelli, M., D'Arcangelo, O., et al. 2010, A&A, 520, A8
Lonsdale, C. J., & Hacking, P. B. 1989, ApJ, 339, 712
López-Caniego, M., González-Nuevo, J., Massardi, M., et al. 2012, MNRAS, submitted [arXiv:1205.1929]
Mandolesi, N., Bersanelli, M., Butler, R. C., et al. 2010, A&A, 520, A3
Marriage, T. A., Baptiste Juin, J., Lin, Y.-T., et al. 2011, ApJ, 731, 100
Marsden, G., Chapin, E. L., Halpern, M., et al. 2011, MNRAS, 417, 1192
Massardi, M., Lopez-Caniego, M., González-Nuevo, J., et al. 2009, MNRAS, 392, 733
Mennella, A., Butler, R. C., Curto, A., et al. 2011, A&A, 536, A3
Murakami, H., Baba, H., Barthel, P., et al. 2007, PASJ, 59, 369
Murdoch, H. S., Crawford, D. F., & Jauncey, D. L., 1973, ApJ, 183, 1
Negrello, M., Magliocchetti, M., Moscardini, L., et al. 2004, MNRAS, 352, 493
Negrello, M., Perrotta, F., González-Nuevo, J., et al. 2007, MNRAS, 377, 1557
Negrello, M., Clemens, M., González-Nuevo, J., et al. 2012, MNRAS, submitted
Neugebauer, G., Habing, H. J., vansDuinen, R., et al. 1984, ApJ, 278, L1
Oliver, S. J., Wang, L., Smith, A. J., et al. 2010, A&A, 518, L21
Patanchon, G., Ade, P. A. R., Bock, J. J., et al. 2009, ApJ, 707, 1750
Pearson, C., & Khan, S. A. 2009, MNRAS, 399, L11
Peel, M. W., Dickinson, C., Davies, R. D., Clements, D. L., & Beswick, R. J. 2011, MNRAS, 416, L99
Planck Collaboration 2011a, A&A, 536, A1
Planck Collaboration 2011b, A&A, 536, A2
Planck Collaboration 2011c, A&A, 536, A7
Planck Collaboration 2011d, A&A, 536, A13
Planck Collaboration 2011e, A&A, 536, A14
Planck Collaboratio 2011f, A&A, 536, A15
Planck Collaboration 2011g, A&A, 536, A16
Planck Collaboration 2011h, A&A, 536, A23
Planck Collaboration 2011i, The Explanatory Supplement to the Planck Early, Release Compact Source Catalogue, ESA
Planck HFI Core Team 2011a, A&A, 536, A4
Planck HFI Core Team 2011b, A&A, 536, A6
Rahmati, A., & van Der Werf, P. P. 2011, MNRAS, 418, 176
Rosset, C., Tristram, M., Ponthieu, N., et al. 2010, A&A, 520, A13
Rowan-Robinson, M. 2009, MNRAS, 394, 117
Rowan-Robinson, M., Broadhurst, T., Oliver, S. J., et al. 1991, Nature, 351, 719
Rowan-Robinson, M., Roseboom, I. G., Vaccari, M., et al. 2010, MNRAS, 409, 2
Sadler, E. M., Ricci, R., Ekers, R. D., et al. 2008, MNRAS, 385, 1656
Scott, S. E., Dunlop, J., & Serjeant, S. 2006, MNRAS, 370, 1057
Serjeant, S., & Harrison, D. 2005, MNRAS, 356, 192
Soifer, B. T., & Neugebauer, G. 1991, AJ, 101, 354
Soifer, B. T., Helou, G., & Werner, M. 2008, ARA&A, 46, 201
Stickel, M., Bogun, S., Lemke, D., et al. 1998, A&A, 336, 116
Takeuchi, T. T., Yoshikawa, K., & Ishii, T. T. 2003, ApJ, 587, L89
Takeuchi, T. T., Ishii, T. T., Dole, H., et al. 2006, A&A, 448, 525
Tauber, J. A., Mandolesi, N., Puget, J., et al. 2010, A&A, 520, A1
Toffolatti, L., Argueso Gomez, F., de Zotti, G., et al. 1998, MNRAS, 297, 117
Tucci, M., Toffolatti, L., de Zotti, G., & Martínez-González, E. 2011, A&A, 533, A57
Valiante, E., Lutz, D., Sturm, E., Genzel, R., & Chapin, E. L. 2009, ApJ, 701, 1814
Vernstrom, T., Scott, D., & Wall, J. V. 2011, MNRAS, 415, 3641
Vieira, J. D., Crawford, T. M., Switzer, E. R., et al. 2010, ApJ, 719, 763
Weiss, A., Ivison, R. J., Downes, D., et al. 2009, ApJ, 705, L45
Wilman, R. J., Jarvis, M. J., Mauch, T., Rawlings, S., & Hickey, S. 2010, MNRAS, 405, 447
Wright, E. L., Chen, X., Odegard, N., et al. 2009, ApJS, 180, 283
Wright, E. L., Eisenhardt, P. R. M., Mainzer, A. K., et al. 2010, AJ, 140, 1868
Zacchei, A., Maino, D., Baccigalupi, C., et al. 2011, A&A, 536, A5

[1] APC, AstroParticule et Cosmologie, Université Paris Diderot, CNRS/IN2P3, CEA/lrfu, Observatoire de Paris, Sorbonne Paris Cité, 10 rue Alice Domon et Léonie Duquet, 75205 Paris Cedex 13, France

[2] Aalto University Metsähovi Radio Observatory, Metsähovintie 114, 02540 Kylmälä, Finland
[3] African Institute for Mathematical Sciences, 6-8 Melrose Road, Muizenberg, Cape Town, South Africa
[4] Agenzia Spaziale Italiana Science Data Center, c/o ESRIN, via Galileo Galilei, Frascati, Italy
[5] Agenzia Spaziale Italiana, viale Liegi 26, Roma, Italy
[6] Astrophysics Group, Cavendish Laboratory, University of Cambridge, J J Thomson Avenue, Cambridge CB3 0HE, UK
[7] Atacama Large Millimeter/submillimeter Array, ALMA Santiago Central Offices, Alonso de Cordova 3107, Vitacura, Casilla 763 0355, Santiago, Chile
[8] CITA, University of Toronto, 60 St. George St., Toronto, ON M5S 3H8, Canada
[9] CNRS, IRAP, 9 Av. colonel Roche, BP 44346, 31028 Toulouse Cedex 4, France
[10] California Institute of Technology, Pasadena, California, USA
[11] Centre of Mathematics for Applications, University of Oslo, Blindern, Oslo, Norway
[12] Centro de Estudios de Física del Cosmos de Aragón (CEFCA), Plaza San Juan, 1, planta 2, 44001 Teruel, Spain
[13] Computational Cosmology Center, Lawrence Berkeley National Laboratory, Berkeley, California, USA
[14] Consejo Superior de Investigaciones Científicas (CSIC), Madrid, Spain
[15] DSM/Irfu/SPP, CEA-Saclay, 91191 Gif-sur-Yvette Cedex, France
[16] DTU Space, National Space Institute, Technical University of Denmark, Elektrovej 327, 2800 Kgs. Lyngby, Denmark
[17] Département de Physique Théorique, Université de Genève, 24 quai E. Ansermet,1211 Genève 4, Switzerland
[18] Departamento de Física Fundamental, Facultad de Ciencias, Universidad de Salamanca, 37008 Salamanca, Spain
[19] Departamento de Física, Universidad de Oviedo, Avda. Calvo Sotelo s/n, Oviedo, Spain
[20] Departamento de Matemáticas, Universidad de Oviedo, Avda. Calvo Sotelo s/n, Oviedo, Spain
[21] Department of Astrophysics/IMAPP, Radboud University Nijmegen, PO Box 9010, 6500 GL Nijmegen, The Netherlands
[22] Department of Physics & Astronomy, University of British Columbia, 6224 Agricultural Road, Vancouver, British Columbia, Canada
[23] Department of Physics and Astronomy, Dana and David Dornsife College of Letter, Arts and Sciences, University of Southern California, Los Angeles, CA 90089, USA
[24] Department of Physics and Astronomy, Tufts University, Medford, MA 02155, USA
[25] Department of Physics, Gustaf Hällströmin katu 2a, University of Helsinki, Helsinki, Finland
[26] Department of Physics, Princeton University, Princeton, New Jersey, USA
[27] Department of Physics, University of California, Berkeley, California, USA
[28] Department of Physics, University of California, One Shields Avenue, Davis, California, USA
[29] Department of Physics, University of California, Santa Barbara, California, USA
[30] Department of Physics, University of Illinois at Urbana-Champaign, 1110 West Green Street, Urbana, Illinois, USA
[31] Department of Statistics, Purdue University, 250 N. University Street, West Lafayette, Indiana, USA
[32] Dipartimento di Fisica e Astronomia G. Galilei, Università degli Studi di Padova, via Marzolo 8, 35131 Padova, Italy
[33] Dipartimento di Fisica e Scienze della Terra, Università di Ferrara, via Saragat 1, 44122 Ferrara, Italy
[34] Dipartimento di Fisica, Università La Sapienza, P. le A. Moro 2, Roma, Italy
[35] Dipartimento di Fisica, Università degli Studi di Milano, via Celoria 16, Milano, Italy
[36] Dipartimento di Fisica, Università degli Studi di Trieste, via A. Valerio 2, Trieste, Italy
[37] Dipartimento di Fisica, Università di Roma Tor Vergata, via della Ricerca Scientifica, 1, Roma, Italy
[38] Dipartimento di Matematica, Università di Roma Tor Vergata, via della Ricerca Scientifica, 1, Roma, Italy
[39] Discovery Center, Niels Bohr Institute, Blegdamsvej 17, Copenhagen, Denmark
[40] Dpto. Astrofísica, Universidad de La Laguna (ULL), 38206 La Laguna, Tenerife, Spain
[41] European Southern Observatory, ESO Vitacura, Alonso de Cordova 3107, Vitacura, Casilla 19001, Santiago, Chile
[42] European Space Agency, ESAC, Planck Science Office, Camino bajo del Castillo, s/n, Urbanización Villafranca del Castillo, Villanueva de la Cañada, Madrid, Spain
[43] European Space Agency, ESTEC, Keplerlaan 1, 2201 AZ Noordwijk, The Netherlands
[44] Haverford College Astronomy Department, 370 Lancaster Avenue, Haverford, Pennsylvania, USA
[45] Helsinki Institute of Physics, Gustaf Hällströmin katu 2, University of Helsinki, Helsinki, Finland
[46] INAF – Osservatorio Astronomico di Padova, Vicolo dell'Osservatorio 5, Padova, Italy
[47] INAF – Osservatorio Astronomico di Roma, via di Frascati 33, Monte Porzio Catone, Italy
[48] INAF – Osservatorio Astronomico di Trieste, via G.B. Tiepolo 11, Trieste, Italy
[49] INAF Istituto di Radioastronomia, via P. Gobetti 101, 40129 Bologna, Italy
[50] INAF/IASF Bologna, via Gobetti 101, Bologna, Italy
[51] INAF/IASF Milano, via E. Bassini 15, Milano, Italy
[52] INFN, Sezione di Roma 1, Universit'a di Roma Sapienza, Piazzale Aldo Moro 2, 00185 Roma, Italy
[53] IPAG: Institut de Planétologie et d'Astrophysique de Grenoble, Université Joseph Fourier, Grenoble 1/CNRS-INSU, UMR 5274, 38041 Grenoble, France
[54] ISDC Data Centre for Astrophysics, University of Geneva, Ch. d'Ecogia 16, Versoix, Switzerland
[55] IUCAA, Post Bag 4, Ganeshkhind, Pune University Campus, 411 007 Pune, India
[56] Imperial College London, Astrophysics group, Blackett Laboratory, Prince Consort Road, London, SW7 2AZ, UK
[57] Infrared Processing and Analysis Center, California Institute of Technology, Pasadena, CA 91125, USA
[58] Institut Néel, CNRS, Université Joseph Fourier Grenoble I, 25 rue des Martyrs, 38041 Grenoble, France
[59] Institut Universitaire de France, 103 bd Saint-Michel, 75005 Paris, France
[60] Institut d'Astrophysique Spatiale, CNRS (UMR 8617) Université Paris-Sud 11, Bâtiment 121, Orsay, France
[61] Institut d'Astrophysique de Paris, CNRS (UMR 7095), 98bis boulevard Arago, 75014 Paris, France
[62] Institut de Ciències de l'Espai, CSIC/IEEC, Facultat de Ciències, Campus UAB, Torre C5 par-2, Bellaterra 08193, Spain
[63] Institute for Space Sciences, Bucharest-Magurale, Romania
[64] Institute of Astronomy and Astrophysics, Academia Sinica, Taipei, Taiwan
[65] Institute of Astronomy, University of Cambridge, Madingley Road, Cambridge CB3 0HA, UK
[66] Institute of Theoretical Astrophysics, University of Oslo, Blindern, Oslo, Norway
[67] Instituto de Astrofísica de Canarias, C/vía Láctea s/n, La Laguna, Tenerife, Spain
[68] Instituto de Física de Cantabria (CSIC-Universidad de Cantabria), Avda. de los Castros s/n, Santander, Spain
[69] Jet Propulsion Laboratory, California Institute of Technology, 4800 Oak Grove Drive, Pasadena, California, USA
[70] Jodrell Bank Centre for Astrophysics, Alan Turing Building, School of Physics and Astronomy, The University of Manchester, Oxford Road, Manchester, M13 9PL, UK
[71] Kavli Institute for Cosmology Cambridge, Madingley Road, Cambridge, CB3 0HA, UK

[72] LAL, Université Paris-Sud, CNRS/IN2P3, Orsay, France
[73] LERMA, CNRS, Observatoire de Paris, 61 avenue de l'Observatoire, Paris, France
[74] Laboratoire AIM, IRFU/Service d'Astrophysique – CEA/DSM – CNRS – Université Paris Diderot, Bât. 709, CEA-Saclay, 91191 Gif-sur-Yvette Cedex, France
[75] Laboratoire Traitement et Communication de l'Information, CNRS (UMR 5141) and Télécom ParisTech, 46 rue Barrault, 75634 Paris Cedex 13, France
[76] Laboratoire de Physique Subatomique et de Cosmologie, Université Joseph Fourier Grenoble I, CNRS/IN2P3, Institut National Polytechnique de Grenoble, 53 rue des Martyrs, 38026 Grenoble Cedex, France
[77] Laboratoire de Physique Théorique, Université Paris-Sud 11 & CNRS, Bâtiment 210, 91405 Orsay, France
[78] Lawrence Berkeley National Laboratory, Berkeley, California, USA
[79] Max-Planck-Institut für Astrophysik, Karl-Schwarzschild-Str. 1, 85741 Garching, Germany
[80] National University of Ireland, Department of Experimental Physics, Maynooth, Co. Kildare, Ireland
[81] Niels Bohr Institute, Blegdamsvej 17, Copenhagen, Denmark
[82] Observational Cosmology, Mail Stop 367-17, California Institute of Technology, Pasadena, CA, 91125, USA
[83] Optical Science Laboratory, University College London, Gower Street, London, UK
[84] SISSA, Astrophysics Sector, via Bonomea 265, 34136, Trieste, Italy
[85] School of Physics and Astronomy, Cardiff University, Queens Buildings, The Parade, Cardiff, CF24 3AA, UK
[86] Space Sciences Laboratory, University of California, Berkeley, California, USA
[87] Stanford University, Dept of Physics, Varian Physics Bldg, 382 via Pueblo Mall, Stanford, California, USA
[88] UPMC Univ Paris 06, UMR7095, 98bis boulevard Arago, 75014 Paris, France
[89] Université de Toulouse, UPS-OMP, IRAP, 31028 Toulouse Cedex 4, France
[90] Universities Space Research Association, Stratospheric Observatory for Infrared Astronomy, MS 211-3, Moffett Field, CA 94035, USA
[91] University of Granada, Departamento de Física Teórica y del Cosmos, Facultad de Ciencias, Granada, Spain
[92] Warsaw University Observatory, Aleje Ujazdowskie 4, 00-478 Warszawa, Poland

Pages 18 to 19 are available in the electronic edition of the journal at http://www.aanda.org

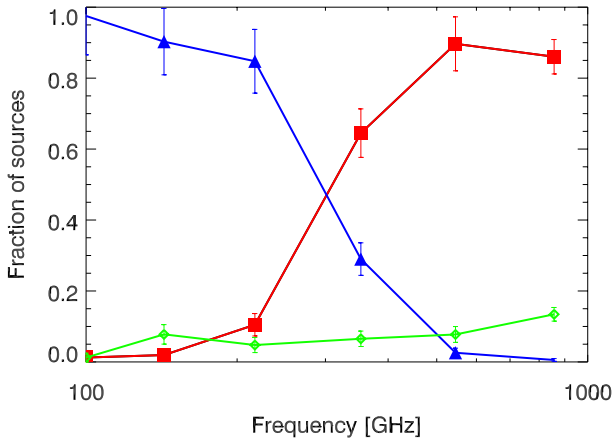

Fig. A.1. As in Fig. 8, the fraction of source type (dusty, red squares; synch, blue triangles) as a function of frequency. The difference is that we have now included the "intermediate" population (green diamonds). We can see that at most 13% of our classification as dusty or synchrotron can be affected by intermediate sources. Our number counts by type (above 80% completeness) are thus almost unaffected by these intermediate type sources.

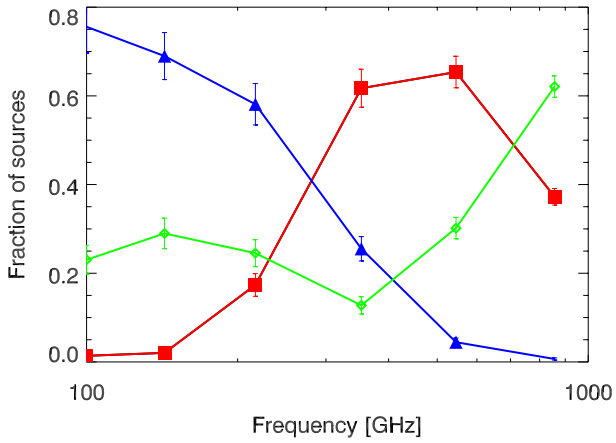

Fig. A.2. Like Fig. A.1, the fraction of source type (dusty, red squares; synchrotron, blue triangles; green diamonds, intermediate) as a function of frequency. The difference is that we have now included the whole catalogue, i.e. including sources affected by more photometric noise below the 80% completeness limit cut. The effect of increasing noise is to induce more sources to be classified as intermediate.

Appendix A: Spectral classification; effect of intermediate sources and photometric noise

In this appendix, we investigate the fate and influence of the so-called "intermediate" sources as defined in Sect. 3.

Figure A.1 shows the fraction of sources (like Fig. 8) by type (dusty, synchrotron, and now intermediate) as a function of frequency computed for sources above 80% completeness. The fraction is at most 13%, and is on average around 7%. The intermediate source population thus has no impact on our number counts by type.

We conclude that a genuine population of intermediate sources exist (i.e. having both a thermal dust emission component and a synchrotron component) but its contribution in number is less than typically 10% (Fig. A.1). Notice that a free-free emission can also play a role in the spectrum flattening around 100 GHz (Peel et al. 2011).

We notice, however, that this intermediate populations lies at the faint end of the flux distribution (i.e. they usually are among the faintest sources of our sample). To investigate further if the presence of intermediate sources is linked to the level of photometric noise, we performed the classification on our whole sample, thus including sources at fluxes below the 80% completeness limit. The results, shown in Fig. A.2, indicates that the higher the photometric noise the more sources are classified as intermediate.

When using the total sample (i.e. with sources fainter that the 80% completeness cut), the fraction of intermediate sources increases, but those sources are always at the faint end of the flux distribution: the effect of the photometric noise is thus mainly responsible for the uncertain classification. This emphasises that we should use highly-complete samples for such statistical analysis, in order not to be biased towards mis-classification.

Appendix B: Some peculiarities; individual sources or groups of sources

While the SEDs of some particular sources have been published in the *Planck* early papers Planck Collaboration (2011e–g), we review here some specific sources detected at low or high frequency, but with unexpected classifications.

B.1. Low-frequency dusty galaxies

There are seven low-frequency sources (three detected at 100 GHz and four at 143 GHz) that are classified as dusty galaxies. This kind of classification is not necessarily expected, unless we detect local galaxies showing both radio and infrared components. For this reason we check them individually.

1) PLCKERC100 G062.69−14.07: there is no radio identification in NVSS & GB6 or in NED, and no detection at LFI frequencies. This source is likely correctly classified as a dusty galaxy.
2) PLCKERC100 G140.41−17.39: this source is found with NED to be NGC 891. There is no LFI detection, but detections in NVSS/GB6. We might be seeing two spectral components (dusty and synchrotron) of this nearby galaxy.
3) PLCKERC100 G141.42+40.57: this is NGC 3034 (M82). As above we are sensitive to both components of this nearby and well-studied galaxy.
4) PLCKERC143 G001.33−20.49: no LFI detection nor radio identification. this source is correctly classified as a dusty galaxy.
5) PLCKERC143 G148.59+28.70: this source is likely a blazar with an almost flat spetrcum at high frequencies and detections in NVSS and GB6. This source is likely incorrectly classified as dusty, because of the small jump in flux at 545 GHz.
6) PLCKERC143 G236.47−14.38: no LFI detection nor radio identification. This source is correctly classified as a dusty galaxy.
7) PLCKERC143 G349.61−52.57: no LFI detection. At 0.2 to 20 GHz it is identified as a flat-spectrum source but its high-frequency spectrum shows a clear dusty behaviour. This source is correctly classified as a dusty galaxy, although a clear radio component is detected.

B.2. High frequency synchrotron galaxies

There are four sources classified at synchrotron sources at 857 GHz. We also check them individually.

1) PLCKERC857 G206.80+35.82: this is a confirmed blazar detected with WMAP. This source is correctly classified as synchrotron-dominated.

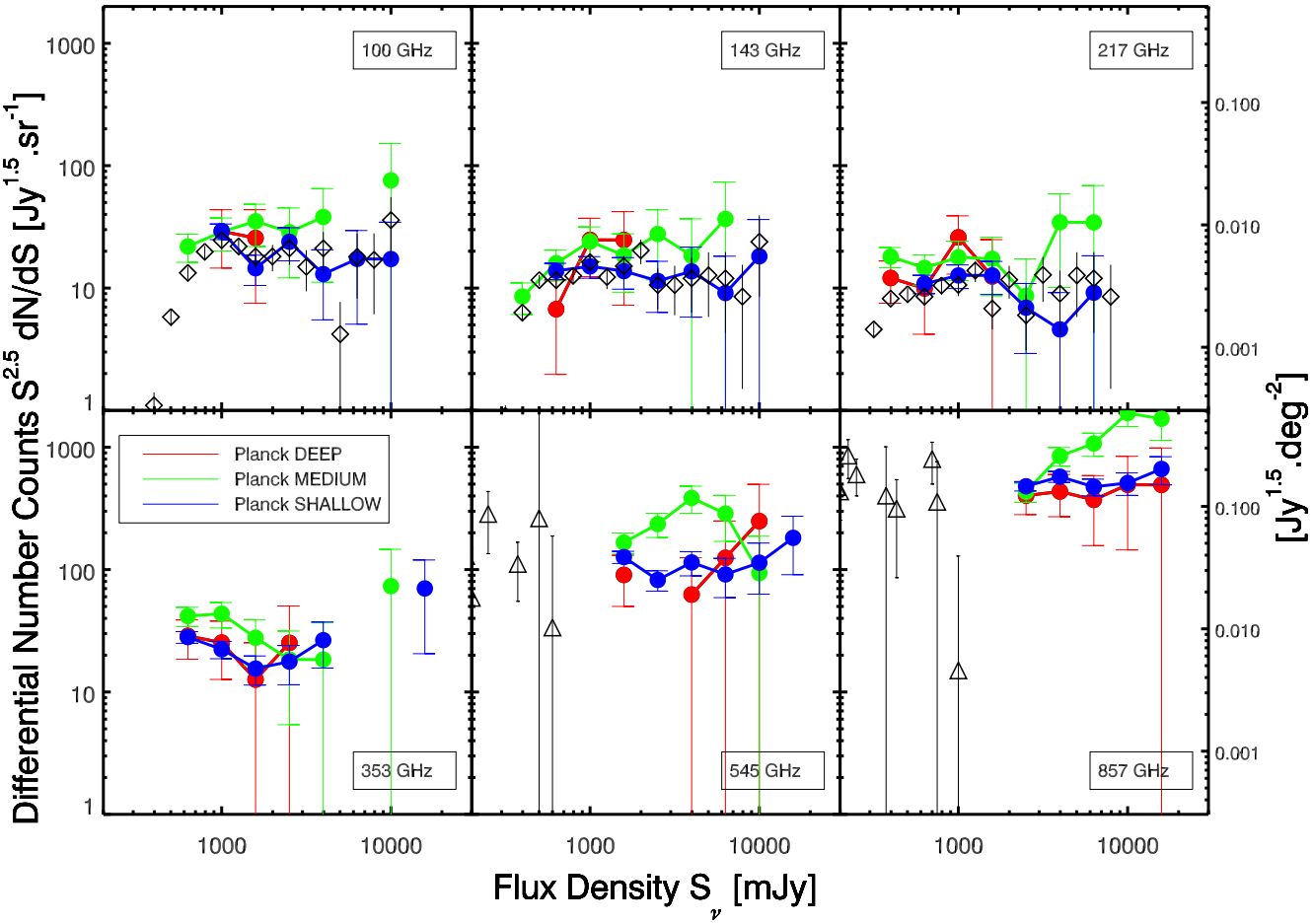

Fig. C.1. *Planck* differential number counts (total, dusty and synchrotron) at 6 frequencies between 100 and 857 GHz, normalized to the Euclidean, for each zone (filled circles): deep (red), medium (green) and shallow (blue). Diamonds are from *Planck* HFI (Planck Collaboration 2011d), triangles from *Herschel* SPIRE (Oliver et al. 2010; Clements et al. 2010) and BLAST Bethermin et al. (2010b). The bump at 4 Jy at 545 GHz (and at 10 Jy at 857 GHz) in the medium zone is discussed in Sect. B.3.

2) PLCKERC857 G237.75−48.48: this is a confirmed blazar detected with WMAP and *ATCA*. This source is correctly classified as synchrotron-dominated.
3) PLCKERC857 G250.08−31.09: this is a confirmed blazar detected with WMAP and *ATCA*. This source is correctly classified as synchrotron-dominated.
4) PLCKERC857 G148.24+52.44: this is NGC 3408, quite faint for *Planck* at high frequencies (812 mJy at 857 GHz and not detected at 545 GHz). This source, although in our sample defined in Sect. 2.3, was not used in the number counts because of the low completeness level at this flux density.

B.3. Bump at 4 Jy at 545 GHz in the medium zone

As discussed in Sect. 4 and shown in Fig. C.1, there is an excess of 545 GHz sources in the medium zone at 4 Jy, which is also seen at 857 GHz at 10 Jy and at 353 GHz at 1 Jy. This bump is created at 545 by 18 sources (between 3 and 5 Jy). Among the sources, we find NGC 3147, NGC 4449, NGC 4217, NGC 3992, NGC 4088, NGC 4096, NGC 4051, NGC 3631, NGC 3938, IC 0750, NGC 4244, NGC 3726, NGC 4214, NGC 7582 and NGC 7552. At 857 GHz, we find 20 sources between 7.6 and 12 Jy, with many in common with the list above. These sources are not physically associated and are spread over a large surface of the sky, although the majority lie around (150 deg, 60 deg) in Galactic coordinates.

Appendix C: Number counts by zone

Figure C.1 shows the number counts for each of the three zones: deep, medium, and shallow. This illustrates the sample variance, as mentioned in Appendix B.3.

Since, with the exception of one zone at 545 GHz, there is little difference between the counts in different zones, this figure also demonstrates that the weight given to each zone in calculating the total number counts has little influence on the result.